nature cell biology

Spatial sequestration of misfolded proteins by a dynamic chaperone pathway enhances cellular fitness during stress

Stéphanie Escusa-Toret[1], Willianne I. M. Vonk[1] and Judith Frydman[1,2]

The extensive links between proteotoxic stress, protein aggregation and pathologies ranging from ageing to neurodegeneration underscore the importance of understanding how cells manage protein misfolding. Using live-cell imaging, we determine the fate of stress-induced misfolded proteins from their initial appearance until their elimination. Upon denaturation, misfolded proteins are sequestered from the bulk cytoplasm into dynamic endoplasmic reticulum (ER)-associated puncta that move and coalesce into larger structures in an energy-dependent but cytoskeleton-independent manner. These puncta, which we name Q-bodies, concentrate different misfolded and stress-denatured proteins en route to degradation, but do not contain amyloid aggregates, which localize instead to the insoluble protein deposit compartment. Q-body formation and clearance depends on an intact cortical ER and a complex chaperone network that is affected by rapamycin and impaired during chronological ageing. Importantly, Q-body formation enhances cellular fitness during stress. We conclude that spatial sequestration of misfolded proteins in Q-bodies is an early quality control strategy occurring synchronously with degradation to clear the cytoplasm of potentially toxic species.

Misfolded proteins challenge the integrity of the cellular proteome and compromise cell viability[1,2]. Their accumulation in insoluble protein aggregates is linked to neurodegenerative amyloid disorders, including Alzheimer's and Huntington's disease[3]. Accordingly, cells evolved elaborating quality control machineries that eliminate misfolded proteins and maintain protein homeostasis[4,5]. Molecular chaperones are central to this process, as they recognize non-native conformations and triage polypeptides for either refolding or degradation through the ubiquitin-proteasome pathway (UPS) or autophagy[4,5]. In addition, cells can actively sequester misfolded proteins in defined quality control compartments[6–8]. Upon proteasome impairment, misfolded proteins partition into spatially and functionally distinct compartments[6,7]: the JUNQ (juxtanuclear quality control) compartment, which sequesters misfolded polypeptides in a detergent-soluble state; and the IPOD (insoluble protein deposit) compartment, which sequesters terminally aggregated polypeptides[9,10]. Amyloid proteins, such as polyQ-expanded Huntingtin, are partitioned primarily to the IPOD, even in the absence of proteasome inhibition[5]. Protein sequestration into these inclusions is proposed as an alternative cellular defense when quality control machineries fail[11–13].

Quality control is viewed as a two-tiered system, whereby misfolded proteins are first either refolded or degraded through the action of chaperones and the UPS, and then, when triage fails, transported in a cytoskeleton-dependent manner to cellular quality control inclusions[14]. By following, in real time, quality control substrates in the absence of proteasome inhibition, we find instead that misfolded proteins are rapidly concentrated in many dynamic inclusions, which we term Q-bodies, even as they are degraded by the proteasome. Q-body formation and movement is independent of the cytoskeleton, but requires the cortical endoplasmic reticulum (ER) and the concerted action of a chaperone network. We propose that sequestration of misfolded proteins is an integral and early aspect of cellular quality control that does not necessarily ensue from proteostasis impairment or cellular dysfunction. Our data have implications for understanding the genesis of terminal protein inclusions characterizing a wide number of human pathologies[1].

RESULTS

Sequestration of misfolded proteins into dynamic puncta is an early quality control response

To understand quality control in unperturbed yeast cells, we used live-cell microscopy to follow the fate of a thermolabile allele of *UBC9* (Ubc9-2 herein Ubc9ts) that is folded at 28 °C (Ubc9ts-N; Fig. 1a) but denatures above 33 °C (Ubc9ts-Den; Fig. 1a,b and Supplementary Fig. S1a)[6]. Ubc9ts–GFP expressed from a galactose-inducible promoter

[1]Department of Biology, Stanford University, Stanford, California 94305, USA.
[2]Correspondence should be addressed to J.F. (e-mail: jfrydman@stanford.edu)

Received 26 November 2012; accepted 7 August 2013; published online 15 September 2013; DOI: 10.1038/ncb2838

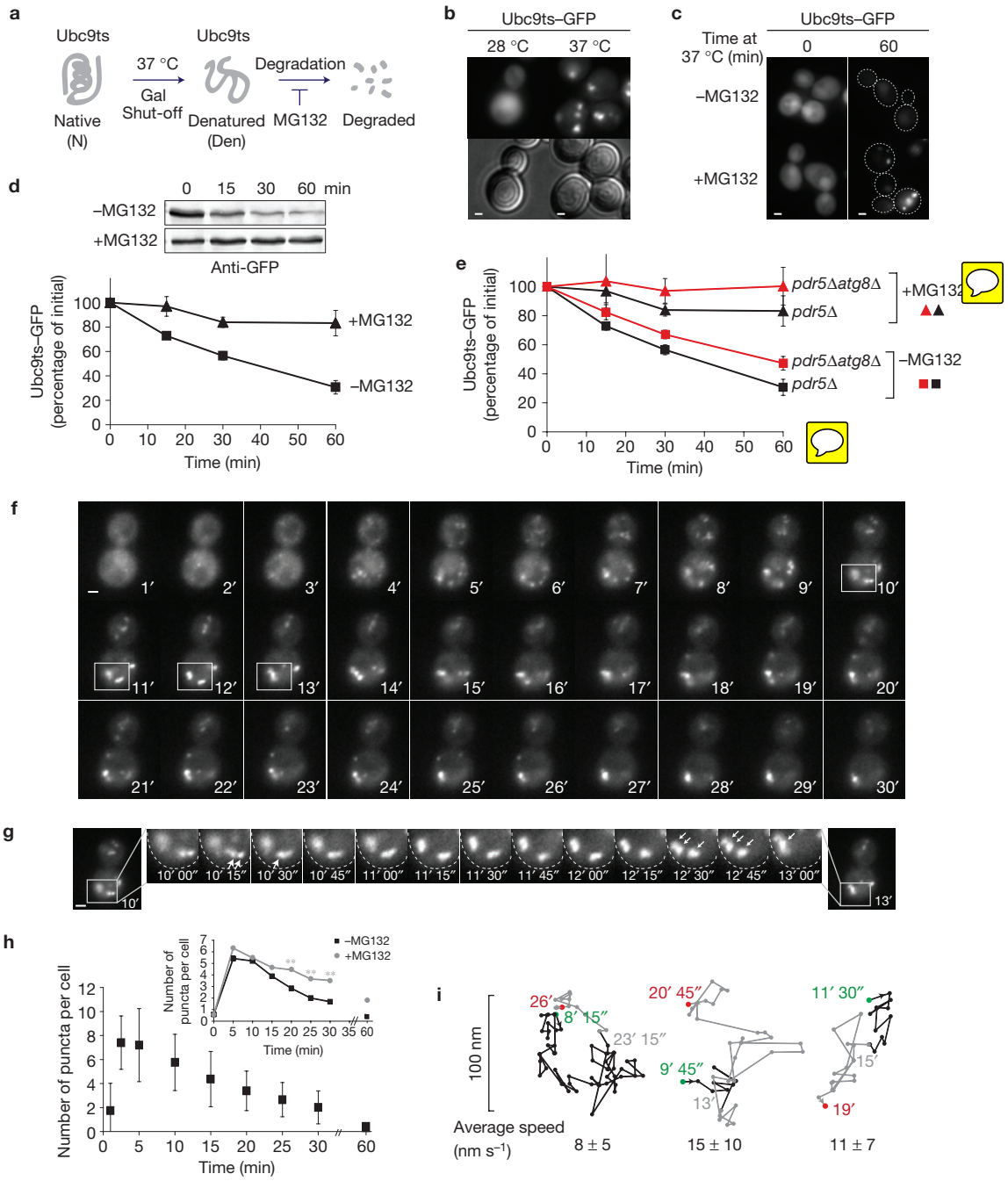

Figure 1 Misfolded proteins are sequestered in Q-bodies upon heat stress. (**a**) Ubc9ts–GFP fate upon heat stress. (**b**) Ubc9ts–GFP-expressing WT cells at 28 °C were shifted to 37 °C for 15 min. GFP (upper panel) and differential interference contrast (lower panel) are shown. (**c**) *pdr5*Δ cells expressing Ubc9ts–GFP were grown at 28 °C in galactose medium and shifted to 37 °C in glucose medium with (+) or without (–) 100 μM MG132. Images show Ubc9ts–GFP at the shift ($t = 0$) and after 60 min ($t = 60$). The dotted lines highlight cell outlines. (**d**) As in **c**, Ubc9ts–GFP was immunoblotted with anti-GFP antibodies and quantified as the relative ratio to the initial amount for each condition. The results represent the mean and standard deviation (s.d.) of three independent experiments. (**e**) *pdr5*Δ and *pdr5*Δ*atg8*Δ cells expressing Ubc9ts–GFP were grown as in **c**. Ubc9ts–GFP was immunoblotted with anti-GFP antibodies (Supplementary Fig. S1b) and quantified relative to the initial amount for each condition. The results represent the mean and s.d. of three independent experiments. (**f**) WT cells expressing Ubc9ts–GFP at 28 °C in galactose medium were shifted to 37 °C in glucose medium. Time series images show GFP signal in a cell 1 min (1′) to 30 min (30′) after the shift (Supplementary Video S1). (**g**) Inset in **f** highlights the coalescence of Ubc9ts–GFP Q-bodies (arrows), from 10 to 13 min after the shift. (**h**) Number of puncta in the medial focal plane over time in WT (main panel; puncta assessed from a total population of $n = 63$ cells over three independent experiments, 1 field counted per experiment) or in *pdr5*Δ cells (puncta assessed from a total population of $n = 36$ cells over three independent experiments, 1 field counted per experiment) with or without MG132 (secondary panel). Results represent mean of puncta for n cells and s.d. $^{**}P < 0.005$, compared with untreated cells for the same indicated time. (**i**) Trajectories of three Ubc9–GFP Q-bodies in WT cells. Positions of particles are represented from each frame of a video (1 frame per 15 s) at the medial focal plane. Consecutive positions are connected by lines: black, before coalescence; grey, after coalescence. Green and red dots indicate the initial and final positions, respectively. Initial, final and coalescing times are indicated, and average speed (±s.d.) over the entire trajectory. Scale bars: 1.5 μm (**b**), 1 μm (**c**,**f**,**g**). Uncropped images of blots are shown in Supplementary Fig. S8.

at 28 °C generated folded Ubc9ts (Ubc9ts-N), localized diffusely throughout the cell. We shut-off Ubc9ts expression by addition of glucose and shifted the cells to 37 °C, causing the pre-existing Ubc9ts to misfold and be degraded with a half-life of approximately 15–20 min (Fig. 1c,d). The UPS is the main degradation pathway for misfolded Ubc9ts because inhibition of autophagy by deletion of Atg8 (ref. 15) produced only a minor stabilization of Ubc9ts (Fig. 1e and Supplementary Fig. S1b). As reported[6], proteasome inhibition leads to Ubc9ts accumulation into the JUNQ and IPOD (Fig. 1c).

The dynamics and fate of misfolded Ubc9ts–GFP during the process of degradation was visualized in live cells by epifluorescence microscopy following expression shut-off (Fig. 1f and Supplementary Video S1). Shortly after shifting to 37 °C, an increasing number of dim scattered Ubc9ts–GFP puncta appeared throughout the cytosol. Within 5 min, 5–10 puncta were clearly observed in the medial focal plane (Fig. 1f). Between 5 and 30 min, the diffuse signal disappeared as the dim Ubc9ts–GFP puncta coalesced into fewer and brighter structures that continued to merge even as Ubc9ts was cleared from the cell (Fig. 1f,g and Supplementary Video S1). Wild-type Ubc9–GFP remained diffuse and soluble at 37 °C and did not form puncta (Supplementary Fig. S1c), confirming that these inclusions arise from Ubc9ts misfolding. Quantification of the average number of puncta in a medial focal plane at 5 min intervals during a 60 min video indicated a consistent decrease in puncta number from 5 to 30 min (Fig. 1h). All puncta disappeared within an hour. Similar results were obtained when Ubc9ts was misfolded at 33 °C, indicating that this pathway is not specific to higher temperature stress (Supplementary Fig. S1a). Upon proteasome inhibition, the formation and early coalescence of Ubc9ts–GFP puncta occur similarly to untreated cells, albeit with a slightly higher number of puncta (Fig. 1h), which continue coalescing into 1–3 large inclusions[6] (Fig. 1c,d). These results suggest that the JUNQ, the IPOD and other inclusions observed upon proteasome inhibition[7] may result from the accumulation of coalesced puncta over time as their clearance is impaired.

We conclude that misfolded proteins do not remain diffusely distributed in the cytosol, but are also not deposited into a static pre-existing compartment. Instead, they are collected and processed through a dynamic cellular pathway into multiple punctate structures throughout the cell that, by coalescence, mature into larger inclusions. By analogy to the dynamic P-body-mediated RNA quality control[16], we propose to name these protein quality control structures Q-bodies.

Q-body dynamics are energy dependent but cytoskeleton independent

Tracking the trajectory of Q-bodies *in vivo* did not reveal any directional movement, suggesting that they do not move on defined tracks (Fig. 1i). The average speed of puncta was 5–15 nm s^{-1}, about 10 times slower than endocytic particles moving on the cytoskeleton[17], and did not change appreciably before (black trace) and after (grey trace) coalescence with another puncta (Fig. 1i). This led us to examine the role of the cytoskeleton on Q-body dynamics. The actin and microtubule cytoskeletons were disrupted with 200 μM latrunculin A (LatA) and 15 μg ml^{-1} nocodazole (Noc), respectively, followed by imaging of Ubc9ts–GFP (Fig. 2a–c top panels). A 10 min LatA treatment before induction of Ubc9ts misfolding completely disrupted the actin cytoskeleton, as confirmed by imaging the actin-binding protein Abp1–GFP (Fig. 2a). Nonetheless, Q-bodies were still formed, processed and degraded in a manner similar to that in the WT (Fig. 2a and Supplementary Video S2). Tracking analysis indicated that LatA treatment did not measurably affect the average speed or directionality of Q-bodies over their lifetime (Fig. 2a, lower panel). Of note, prolonged incubation (2 h) with LatA did perturb Q-body formation and movement (Fig. 2b), suggesting that prolonged disruption of the actin cytoskeleton impairs protein homeostasis. The tubulin cytoskeleton is also dispensable for Q-body formation and dynamics. Treatment with Noc for 10 min disrupted microtubules, but did not affect Q-body dynamics and clearance (Fig. 2c). We conclude that neither Q-body formation nor dynamics requires a functional actin and tubulin cytoskeleton.

We next assessed whether Q-body formation and movement require energy. Intracellular ATP depletion with sodium azide and deoxyglucose for 30 min (Fig. 2d) did not abrogate Q-body formation, suggesting that this step is energy independent. However, Q-body dynamics, coalescence and clearance were highly perturbed (Fig. 2d and Supplementary Video S3). We conclude that the concentration of misfolded protein into Q-bodies is energy independent, whereas their movement, coalescence and clearance require ATP.

Q-body formation and processing requires an intact cortical ER

We next sought to identify cellular structures associated with Q-bodies. As the JUNQ co-localizes with the perinuclear ER (ref. 6), Ubc9ts was co-expressed with the nuclear marker Npl3, or with the perinuclear ER protein Hmg1 (Fig. 3a,b)[18]. *Z*-sections of deconvolved images revealed the distribution of Ubc9ts Q-bodies vis-à-vis the nucleus (Fig. 3a,b). In each cell analysed, at least one puncta was juxtanuclear, whereas the others were distributed throughout the cell.

No obvious co-localization of Q-bodies was observed with early endosomes (GFP–Snc1), late endosomes (GFP–Pep12), the vacuole (MDY64), autophagic structures (CHFP–Atg8) and the spindle pole body (Spc42–GFP; Supplementary Fig. S2a,b). Given the vicinity of one inclusion with the perinuclear ER, we examined Q-body association with the cortical ER, extending as a tubular network throughout the cell[19]. Two-colour *Z*-stacks of deconvolved images from cells expressing Ubc9ts–CHFP and the cortical ER marker Rtn1–GFP revealed a close proximity between Q-bodies and cortical ER tubules (Fig. 3c,d and Supplementary Video S4).

The role of the cortical ER in Q-body dynamics was assessed in *rtn1*Δ*rtn2*Δ*yop1*Δ cells, whose cortical ER morphology is disrupted[20–22]. A large Ubc9ts inclusion was already observed at the permissive temperature (Fig. 3e). At 37 °C, a few additional dim puncta appeared and coalesced with the large inclusion (Fig. 3e and Supplementary Video S5). After 30 min at 37 °C, when most misfolded Ubc9ts was cleared in WT cells, the large inclusion persisted in over 50% of *rtn1*Δ*rtn2*Δ*yop1*Δ cells, consistent with a delay in Ubc9ts degradation (Fig. 3f). Thus, the formation, dynamics and clearance of cytoplasmic Q-bodies rely on the integrity of a dynamic ER network (Fig. 3g).

The Hsp70–Hsp90 chaperone network mediates Q-body formation and clearance

The ATP-dependence of Q-body clearance resonates with previous data implicating the ATP-dependent heat-shock protein 70 (Hsp70) and

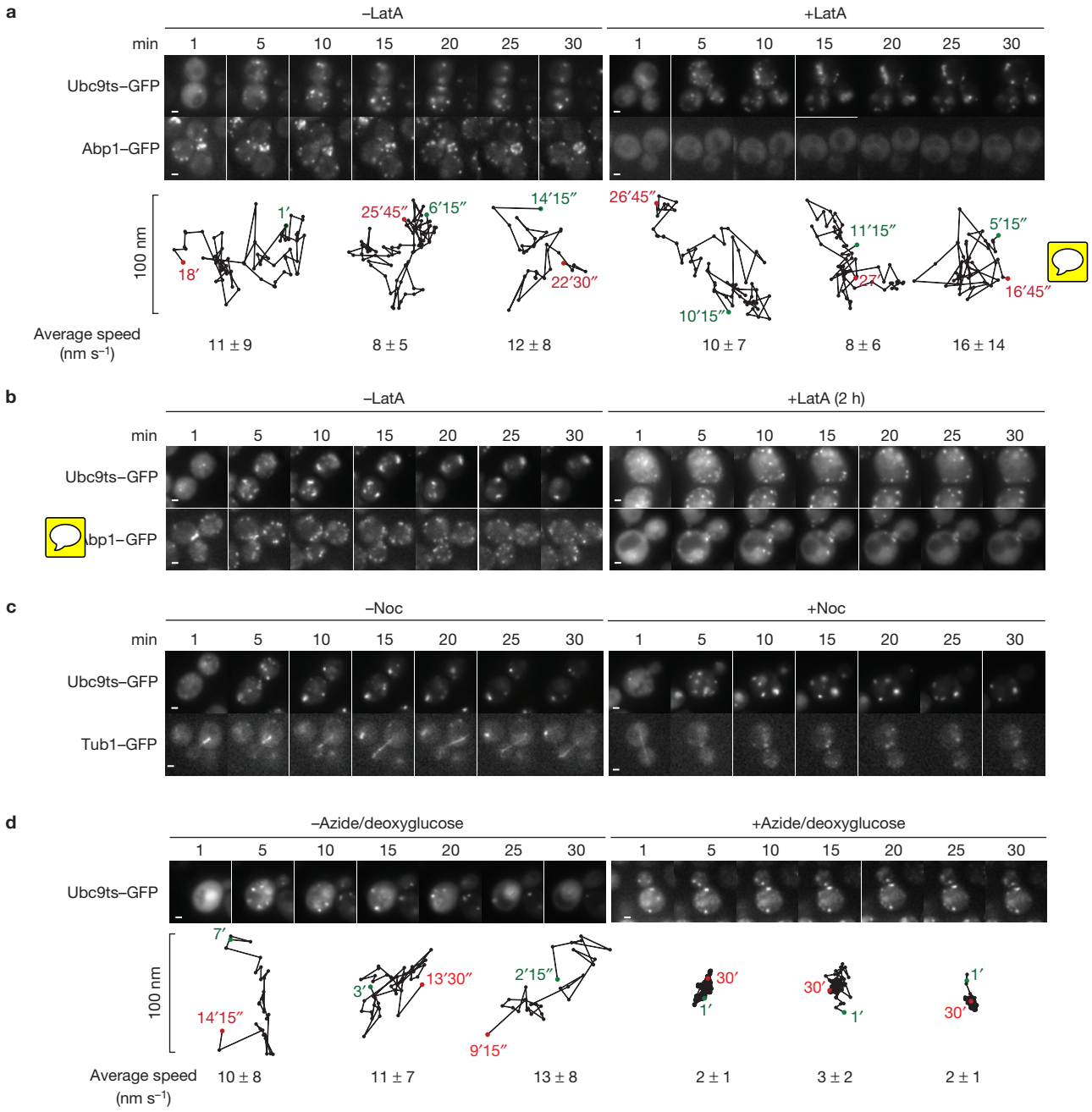

Figure 2 Energy dependency but cytoskeleton independency of Q-body dynamics. (**a**) WT cells expressing Ubc9ts–GFP (top row of images) or Abp1–GFP (bottom row of images) were grown at 28 °C in galactose medium and treated with (right panel) or without (left panel) 200 μM LatA for 10 min before a shift to 37 °C in glucose medium. Five-minute series of images show Ubc9ts–GFP or Abp1–GFP signal (Supplementary Video S2). Trajectories of three Ubc9–GFP puncta in WT cells with or without LatA are represented (bottom panel) as described in Fig. 1i. (**b**) WT cells expressing Ubc9ts–GFP and Abp1–GFP were grown as in **a** but treated with (right panel) or without (left panel) LatA for 2 h before the shift. (**c**) WT cells expressing Ubc9ts–GFP or Tub1–GFP were grown as in **a** but treated with (right panel) or without (left panel) 15 μg ml^{-1} Noc for 10 min before the shift. Five-minute series of images show Ubc9ts–GFP or Tub1–GFP signal. (**d**) WT cells expressing Ubc9ts–GFP were grown as in **a** but treated for 30 min with (right panel) or without (left panel) 10 mM azide and deoxyglucose before the shift. Five-minute series of images show Ubc9ts–GFP signal (Supplementary Video S3). Trajectories of three Ubc9–GFP puncta in cells with and without azide and deoxyglucose treatment are represented (lower panel) as described in Fig. 1i. Scale bars, 1 μm.

Hsp90 systems in misfolded protein quality control (Supplementary Table S1)[23–27]. Indeed, Hsp70, Hsp90 and the Hsp70 cofactor, the Hsp110 chaperone Sse1, are also required for degradation of misfolded Ubc9ts (Fig. 4b). At 37 °C, the Hsp70 Ssa1 co-localized with all misfolded Ubc9ts Q-bodies (Fig. 4a). The role of Hsp70 in the Q-body pathway was examined using two Hsp70-deficient strains: *ssa1*Δ*ssa2*Δ, lacking the two major SSA isoforms, and *ssa1ts ssa2*Δ*ssa3*Δ*ssa4*Δ, containing a single temperature-sensitive SSA isoform and lacking the others[28]. Both strains yielded similar results (Fig. 4c and Supplementary Fig. S3b). Even before the temperature shift, most cells contained a static bright cortical inclusion, indicating that Hsp70 contributes to conformational maintenance of Ubc9ts–GFP at the permissive

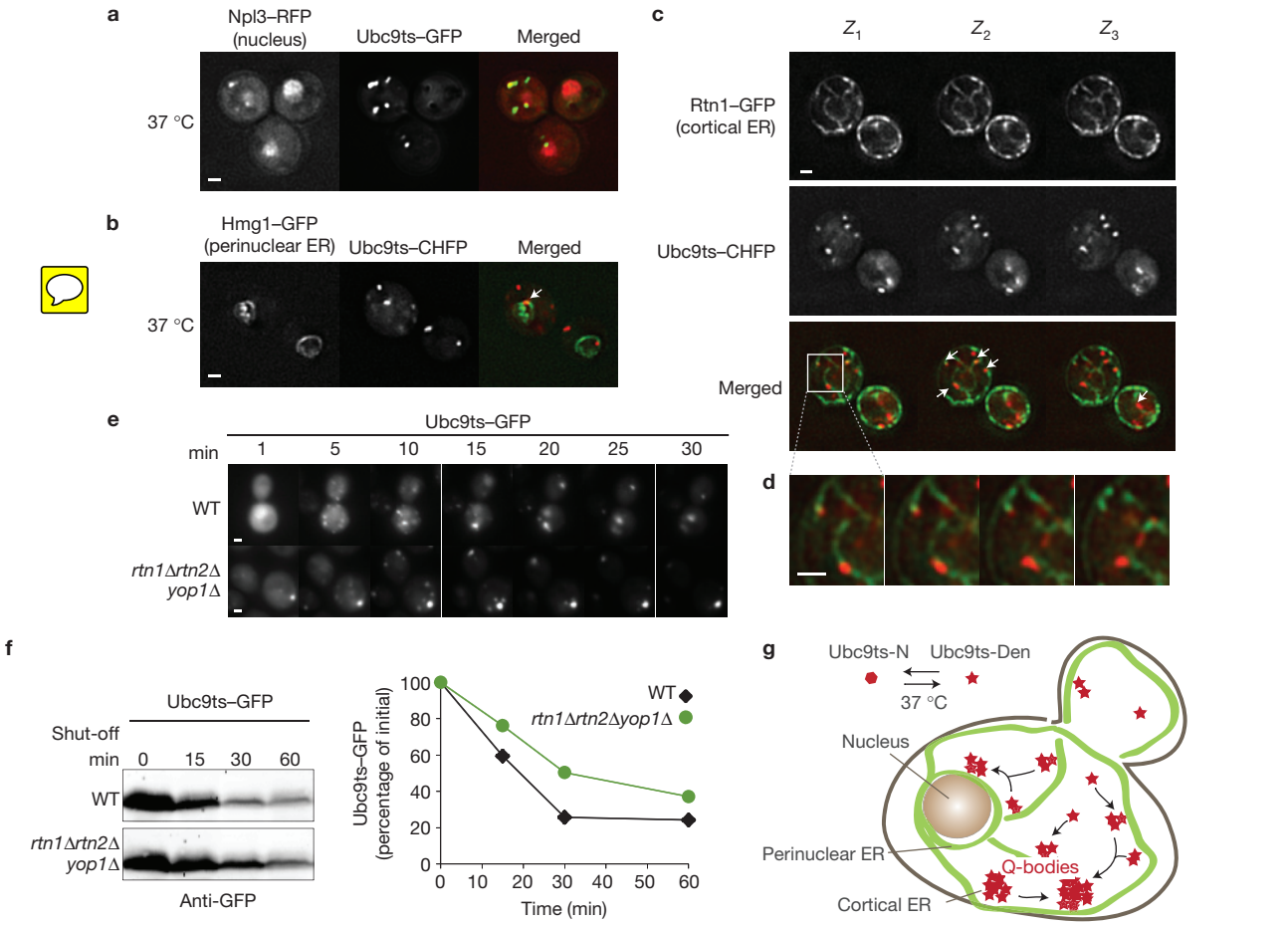

Figure 3 Q-body dynamics relies on an intact cortical ER. (**a**) Cells expressing Npl3–RFP and Ubc9ts–GFP were imaged after 10 min at 37 °C. Two-colour deconvolved images show Npl3–RFP signal (nucleus) in red and Ubc9ts–GFP signal in green. (**b**) Cells expressing Hmg1–GFP (perinuclear ER, green) and Ubc9ts–CHFP (red) were imaged as in **a**. Arrow indicates Q-body in proximity to the ER. (**c**) Cells expressing Rtn1–GFP and Ubc9ts–CHFP were imaged after 10 min at 37 °C. Two-colour images of three *Z*-focal plans (0.2 μm intervals) show Rtn1–GFP signal (cortical ER) in green and Ubc9ts–CHFP signal in red (Supplementary Video S4). Arrows indicate Q-bodies in proximity to the cortical ER. (**d**) Inset from **c** representing a series of 0.2 μm *Z*-sections. (**e**) Ubc9ts–GFP was expressed in WT and rnt1Δ*rtn2*Δ*yop1*Δ cells at 28 °C in galactose medium and the cells were shifted to 37 °C in glucose medium. Five-minute series of images show Ubc9ts–GFP signal over 30 min. (**f**) As in **e**, cells were collected at the indicated times from the shift and Ubc9ts–GFP was immunoblotted with anti-GFP antibodies. Ubc9ts–GFP was quantified as the relative ratio to the initial amount from one experiment representative of four independent experiments. (**g**) Schematic of ER-associated Q-body processing of misfolded Ubc9ts (red star). Green represents the ER network throughout the cell. Scale bars: 1 μm. Uncropped images of blots are shown in Supplementary Fig. S8.

temperature (Fig. 4c and Supplementary Video S6). After the shift, the number of puncta remained unchanged over 30 min: no coalescence of the faint additional puncta was detected and most of the misfolded protein was found in the large inclusion (Fig. 4c,d). Thus, Hsp70 is required for Q-body formation, maturation and clearance, consistent with biochemical experiments (Fig. 4b). Q-bodies still formed in Hsp90-deficient cells (*hsc82*Δ*hsp82ts*)[25], but their movement and coalescence were markedly affected, associated with a strong defect in misfolded Ubc9ts–GFP degradation (Fig. 4b,e,f and Supplementary Video S7). Thus, Hsp90 also participates in Q-body dynamics and degradation, but acts after the initial formation of inclusions.

The activity of Hsp70 and its cooperation with Hsp90 is regulated by J-domain proteins (Supplementary Fig. S3a). As Ydj1 is ER-associated through a farnesyl group[29], we examined whether it helps to process ER-associated Q-bodies. *ydj1*Δ cells contained more diffuse misfolded Ubc9ts than WT cells and numerous dim puncta at the periphery (Fig. 4g). Cells expressing the farnesylation-defective mutant *ydj1*(C406S) (ref. 30) also exhibited clusters of tiny cortical puncta that seemed unable to merge, suggesting a defect in Q-body coalescence (Fig. 4g and Supplementary Video S8). However, Ubc9ts was eventually degraded with similar kinetics as the WT (Fig. 4g and Supplementary Video S8 and Supplementary Fig. S3c), perhaps owing to the high level of redundancy between J-domain proteins[31]. Indeed, disruption of both Ydj1 and another ER-anchored J-domain protein, Hlj1, in the *hlj1*Δ*ydj1*–151 strain[32] strongly affected Q-body formation. Only faint Ubc9ts–GFP puncta were discernible in *hlj1*Δ*ydj1*–151 cells at 37 °C (Supplementary Fig. S3d). Thus, ER-anchored J-domain proteins, but perhaps also other homologues, participate in Q-body formation. The Hsp70 nucleotide exchange factor Sse1 also affected Q-body dynamics (Fig. 4h and Supplementary Video S6). *sse1*Δ cells exhibited a significant delay in Q-body clearance, associated with Ubc9ts degradation impairment (Fig. 4b and Supplementary Fig. S3e). We conclude that a chaperone network involving Hsp70, Hsp90 and their co-chaperones mediates the active formation and

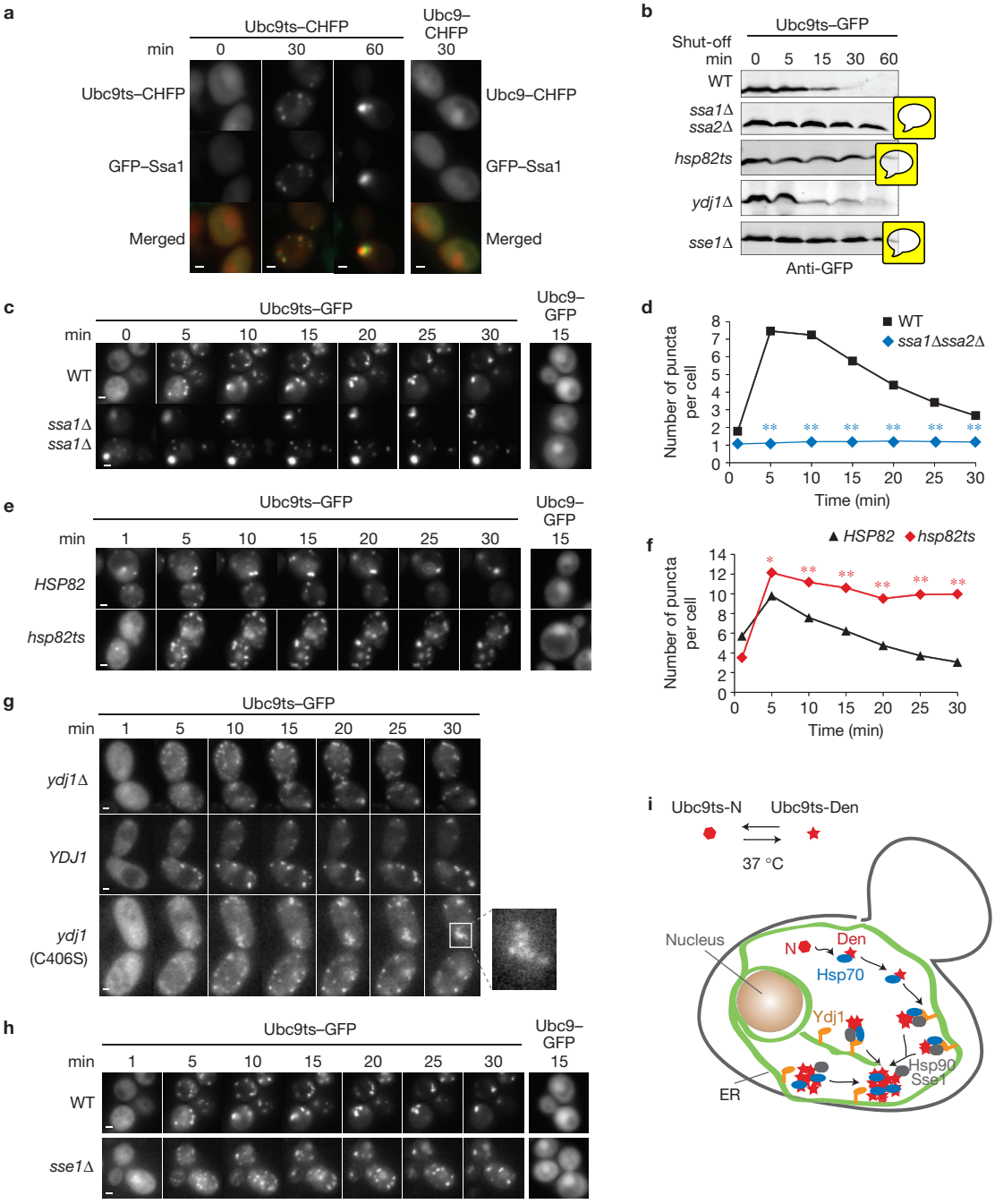

Figure 4 The maturation and degradation of Q-bodies rely on the Hsp70–Hsp90 system. (**a**) WT cells co-expressing GFP–Ssa1 and Ubc9ts–CHFP, or GFP–Ssa1 and Ubc9–CHFP, were grown at 28 °C in galactose medium and shifted to 37 °C in glucose medium. Two-colour images show GFP–Ssa1 signal in green and Ubc9ts–CHFP signal in red at 0, 30 and 60 min after the shift. Cells expressing Ubc9–CHFP and GFP–Ssa1 were imaged 30 min after the shift. (**b**) Cells expressing Ubc9ts–GFP at 28 °C in galactose medium were shifted to 37 °C ($t = 0$) in glucose medium. Cells were collected at the indicated times and Ubc9ts–GFP immunoblotted using anti-GFP antibodies. (**c**) Ubc9ts–GFP was expressed in WT and *ssa1*Δ*ssa2*Δ cells at 28 °C in galactose medium and the cells were shifted to 37 °C in glucose medium. Five-minute series of images show Ubc9ts–GFP signal over 30 min. Cells expressing Ubc9–GFP were similarly prepared and imaged 15 min after the shift. (**d**) Average number of puncta per cell in WT (black squares) and *ssa1*Δ*ssa2*Δ (blue diamonds) cells over time. Puncta assessed from a total population of $n = 35$ cells over three independent experiments (1 field counted per experiment). $^{**}P < 0.005$, compared with WT for the same indicated time. (**e**) WT and *hsp82ts* cells expressing Ubc9ts–GFP or Ubc9–GFP were prepared and imaged as in **c**. (**f**) Average number of puncta per cell in WT (black triangles) and *hsp82ts* (red diamonds) cells over time. Puncta assessed from a total population of $n = 25$ cells over two independent experiments (1 field counted per experiment). $^{*}P < 0.05$, $^{**}P < 0.005$, compared with WT for the same indicated time. (**g**) *ydj1*Δ strains expressing Ubc9ts–GFP alone, and in combination with *YDJ1*, *ydj1*(C406S) or empty vector were prepared and imaged as in **c**. The inset shows a *ydj1*(C406S)-expressing cell. (**h**) WT or *sse1*Δ cells expressing Ubc9ts–GFP or Ubc9–GFP were prepared and imaged as in **c**. (**i**) Role of the Hsp70–Hsp90–Hsp110 system in the Q-body pathway for misfolded Ubc9ts (red star). Green represents the ER network throughout the cell. Scale bars: 1.5 μm (**a**), 1 μm (**c**,**e**,**g**,**h**). Uncropped images of blots are shown in Supplementary Fig. S8.

maturation of Q-bodies, as well as their degradation (Fig. 3i and Supplementary Table S1).

Balance between addition and dissolution activities controls Q-body dynamics

We next examined the role of the disagregase Hsp104 and the small heat shock proteins (HSPs) implicated in prion formation[33,34] and aggregate management in proteasome-inhibited cells[6,7,14]. Live-cell imaging demonstrated that both Hsp104 and Hsp42 associate with Ubc9ts–CHFP Q-bodies formed upon heat stress (Fig. 5a–c and Supplementary Video S9). At 37 °C, in the absence of proteasome inhibition, Hsp104 and Hsp42 persist in the punctate Q-bodies structures even after Ubc9ts–CHFP degradation (Fig. 5a and Supplementary Video S9), suggesting that endogenous heat-denatured proteins are also concentrated and processed through the Q-body pathway. Accordingly, cells not expressing Ubc9ts, or expressing native Ubc9–CHFP, also formed Hsp104–GFP- and Hsp42–GFP-containing puncta upon heat stress, which move and coalesce with similar dynamics as Ubc9ts Q-bodies (Fig. 5b,c). We conclude that Hsp42 and Hsp104 are components of endogenous Q-bodies, which form upon heat stress as a physiological response to misfolded proteins.

Interestingly, untreated and proteasome-inhibited cells exhibited differences in their Hsp104 and Hsp42 distribution. In untreated cells, Hsp42–GFP co-localized with all of the Ubc9ts-containing puncta (Fig. 5c), whereas in proteasome-inhibited cells, Hsp42 was absent from some inclusions[7]. Hsp104 did not co-localize with perinuclear puncta without proteasome inhibitor (Fig. 5b). The lack of Hsp104 in perinuclear puncta was confirmed by two-colour *Z*-stack deconvolution and analysis of DAPI (4′,6-diamidino-2-phenylindole)-labelled fixed cells (Supplementary Fig. S4). Possibly, proteasome inhibition alters inclusion dynamics and composition, as inclusions continue coalescing and persist much longer in the cell.

We evaluated how Hsp104 and the small HSPs Hsp42 and Hsp26 participate in Q-body processing. In *hsp26*Δ cells, the inclusion dynamics and Ubc9ts half-life were unaffected (Fig. 5d–f). In *hsp104*Δ cells, misfolded Ubc9ts–GFP progressed from dim puncta to the formation of medium-intensity puncta, as in WT cells. These medium-intensity puncta did not coalesce into few brighter inclusions as in WT cells, indicating that the progression of the pathway is blocked by loss of Hsp104 (Fig. 5d,e and Supplementary Video S10). In *hsp42*Δ, only a few dim puncta formed after 10 min indicating a severe defect in Q-body formation (Fig. 5d and Supplementary Video S10). Remarkably, Ubc9ts degradation was unaffected in both *hsp104*Δ and *hsp42*Δ strains (Fig. 5f). Thus, sequestration into larger inclusions is not essential for misfolded protein degradation.

The fact that puncta coalescence, but not degradation, requires a disaggregase such as Hsp104 is counter-intuitive; a simple model would predict that disaggregase deletion leads to formation of larger hard-to-degrade inclusions. We reasoned that puncta coalescence may involve Hsp104-mediated dissolution of some puncta followed by re-addition of the released misfolded protein into existing inclusions (Fig. 5i). In this view, loss of puncta in *hsp42*Δ cells would not reflect an absolute requirement of Hsp42 for Q-body formation but rather a shift in the balance between Hsp42-stimulated addition and Hsp104-stimulated dissolution. Indeed, Ubc9ts inclusions were observed in the double *hsp42*Δ*hsp104*Δ cells (Fig. 5g and Supplementary Video S10), indicating that Hsp42 is not required for inclusion formation. However, puncta intensity in *hsp42*Δ*hsp104*Δ was heterogeneous and their coalescence was affected, consistent with Hsp104 promoting Q-body maturation into large inclusions. Notably, Ubc9ts degradation was unaffected in *hsp42*Δ*hsp104*Δ cells (Fig. 5f). Hsp104 is not the only chaperone promoting Q-body dissolution, because the *hsp42*Δ*sse1*Δ mutant also forms inclusions (Fig. 5h), albeit with severely affected dynamics. Thus, a chaperone-mediated balance between addition and dissolution regulates Q-body formation and maturation (Fig. 5i).

Soluble misfolded proteins, but not amyloidogenic IPOD substrates, transit through the Q-body pathway

The generality of the Q-body pathway was assessed by co-expressing Ubc9ts with two distinct quality control substrates: misfolded variants of the tumour suppressor VHL or the thermolabile firefly luciferase (Luc)[25,35]. These misfolded proteins also formed Q-bodies indistinguishable from those observed for Ubc9ts. The puncta formed by VHL or Luc completely co-localized with Ubc9ts Q-bodies, moved and coalesced together throughout the time course of degradation (Fig. 6a,b and Supplementary Video S11 and Supplementary Fig. S5a). Importantly, VHL did not co-localize non-specifically with WT Ubc9, which remains folded at 37 °C (Fig. 6a). VHL puncta were generated regardless of the presence of Ubc9 and proceeded through the Q-body pathway (Supplementary Fig. S5b). This indicates that different misfolded proteins are recruited to the same cellular structures and are handled by the same quality control pathway.

We examined whether the Q-body pathway overlaps with insoluble amyloidogenic IPOD substrates such as the prion Rnq1 and the polyglutamine-expanded Huntingtin exon 1 fragment, Htt-Q97 (Fig. 6e)[6]. Live-cell imaging of misfolded Ubc9ts or VHL in cells co-expressing either Htt-Q97 or Rnq1 indicated that most Ubc9ts or VHL puncta moved and evolved independently of the IPOD. A few dim puncta transiently co-localized with the IPOD, but without merging with it (Fig. 6c,d and Supplementary Video S11 and S5c). Notably, Q-body dynamics were slightly altered in the presence of Htt-Q97 or Rnq1, suggesting that the presence of amyloids in the IPOD can affect protein homeostasis. Ubc9ts and VHL were still cleared, whereas Rnq1 and Htt-Q97 persisted for the duration of the time course (Fig. 6c,d and Supplementary Video S11 and S5c). These results reveal two main fates for misfolded proteins in the absence of proteasome inhibition.

Distinct role of chaperones in Q-body and IPOD formation

The different mechanisms to cope with misfolded proteins could stem from their distinct interactions with the chaperone machinery. Indeed, chaperones participate differently in Q-body and IPOD formation, both qualitatively (Fig. 6f) and when quantifying the number of cells with inclusions over the population (Fig. 6g,h). Q-body substrates formed one main inclusion in *ssa1*Δ*ssa2*Δ cells; large peripheral inclusions in *hsp104*Δ cells; and no inclusions in *hsp42*Δ cells. In contrast, IPOD substrates did not form any inclusions in *hsp104*Δ mutant as described previously[36–38], and significantly fewer inclusions in *ssa1*Δ*ssa2*Δ cells (Fig. 6f,h). Unlike Q-bodies, IPOD inclusions were still formed in *hsp42*Δ mutant cells, even though they seemed dimmer (Fig. 6f). Hsp42 did not co-localize with the IPOD substrates in non-stressed cells, and weakly at higher temperatures (Supplementary Fig. S5d,e), consistent with it being

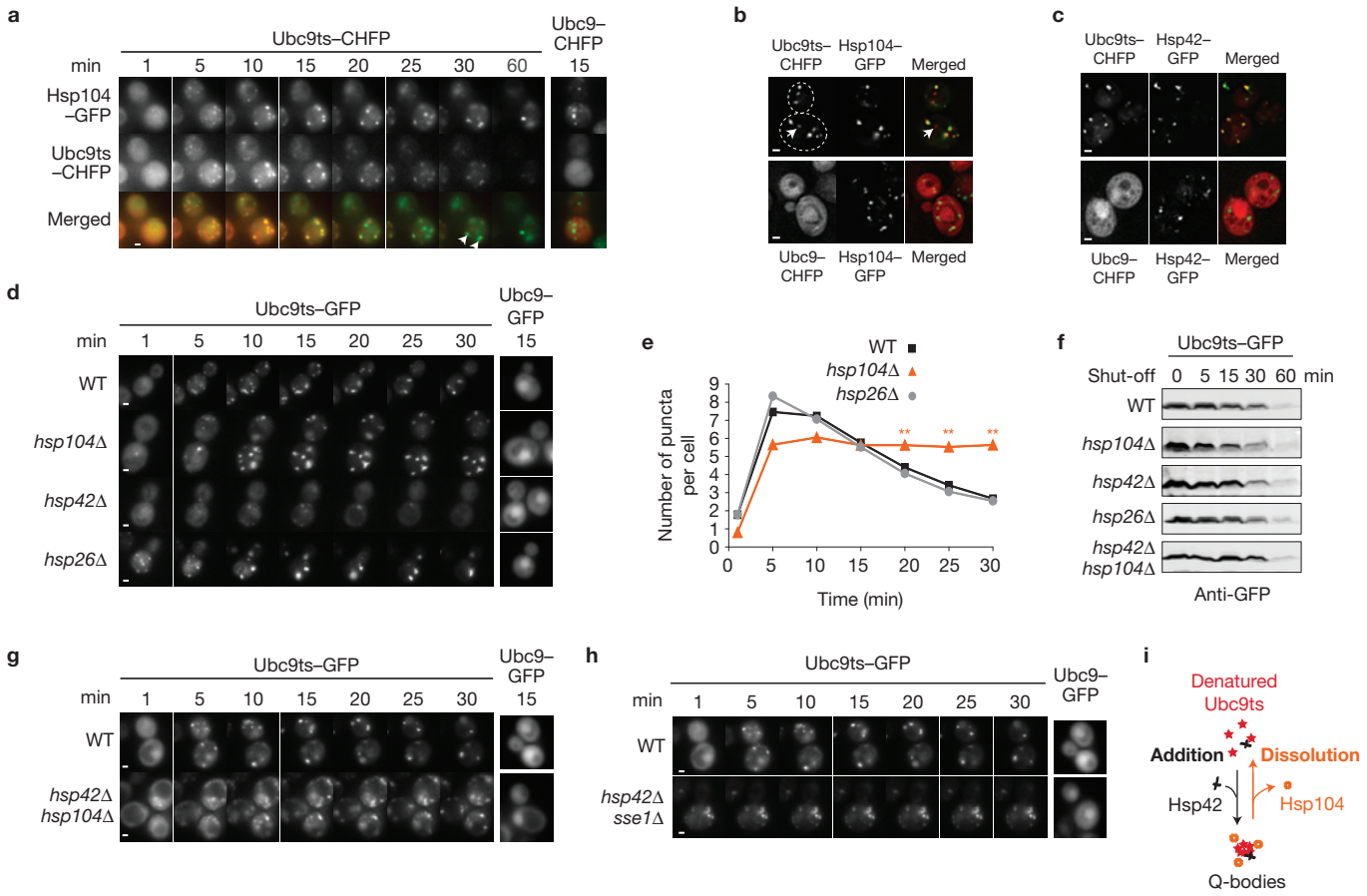

Figure 5 Balance between addition and dissolution activities controls Q-body dynamics. (**a**) Cells expressing Hsp104–GFP and Ubc9ts–CHFP or Ubc9–GFP were grown at 28 °C in galactose medium and shifted to 37 °C in glucose medium. Five-minute series of a two-colour video show Hsp104–GFP signal in green and Ubc9ts–CHFP signal in red over 60 min. Cells expressing Hsp104–GFP and Ubc9–CHFP were imaged 15 min after the shift. (**b**) As in **a**, but cells were imaged 10 min after the shift. Two-colour deconvolved images show Hsp104–GFP signal in green and Ubc9ts–CHFP or Ubc9–CHFP signal in red. (**c**) Cells expressing Hsp42–GFP (green) and Ubc9ts–CHFP or Ubc9–CHFP (red) were imaged as in **b**. (**d**) WT, hsp104Δ, *hsp42*Δ and *hsp26*Δ cells expressing Ubc9ts–GFP or Ubc9–GFP were prepared as in **a**. Five-minute series of images show Ubc9ts–GFP signal over 30 min. Ubc9–GFP signal is shown 15 min after the shift. (**e**) Average number of puncta per cell in the WT (black squares), *hsp104*Δ (orange triangles) and *hsp26*Δ (grey circles) strains over time. Puncta assessed from a total population of $n = 35$ cells over three independent experiments (1 field counted per experiment). $^{**}P < 0.005$, compared with WT for the same indicated time. (**f**) The indicated strains expressing Ubc9ts–GFP were grown as in **a** and collected at the indicated times from the shift ($t = 0$). Ubc9ts–GFP was immunoblotted using anti-GFP antibodies. (**g**) WT and *hsp42*Δ*hsp104*Δ cells expressing Ubc9ts–GFP and Ubc9–GFP were prepared and imaged as in **d**. (**h**) WT and the *hsp42*Δ*sse1*Δ cells expressing Ubc9ts–GFP and Ubc9–GFP were prepared and imaged as in **d**. (**i**) Dissolution–addition balance between Hsp104 and Hsp42: Q-body coalescence results from an Hsp104-mediated process of dissolution followed by Hsp42 stimulated re-addition of the released misfolded protein into existing inclusions. Scale bars: 1 μm. Uncropped images of blots are shown in Supplementary Fig. S8.

dispensable for IPOD formation. This may reflect the higher tendency of amyloidogenic proteins to self-assemble. Alternatively, IPOD substrates may be less dependent on the action of Hsp42 because they are more refractory to the disaggregase activity of Hsp104 and other chaperones.

Q-bodies arise in response to proteotoxic stress

We next examined whether Q-bodies arise generally upon proteotoxic stress. Cells were exposed to ethanol, which denatures pre-existing proteins[39], or treated with the proline analogue azetidine 2-carboxylic acid (AZC), which causes misfolding when incorporated into newly synthesized proteins[40]. Exposure at 37 °C served as a positive control (Fig. 7a). Ubc9ts–GFP and Hsp104–GFP were used to visualize Q-bodies. Ethanol treatment was sufficient to generate Hsp104–GFP- and Ubc9ts–GFP-positive Q-bodies similar to those observed during heat stress (Fig. 7a). Although their kinetics of appearance was faster during heat stress, Q-body dynamics and coalescence seemed similar in all treatments (Fig. 7a).

We determined whether generating newly synthesized misfolded proteins affects the state of pre-existing folded proteins. Synthesis of Ubc9ts was repressed by glucose addition at 28 °C, yielding a pool of pre-existing folded and diffusely localized Ubc9ts, which served as a sensor of general proteostasis in the cell. Newly translated misfolded proteins were generated by AZC treatment at 28 °C. Strikingly, the pre-existing folded Ubc9ts–GFP re-localized to Q-bodies at 28 °C after AZC addition, even though no new Ubc9ts protein was being translated (Fig. 7a). These results indicate that misfolding of newly made proteins shifts the proteostasis balance of the cell to induced misfolding of a pre-existing labile protein, probably because its folding depends on the continued action of chaperones.

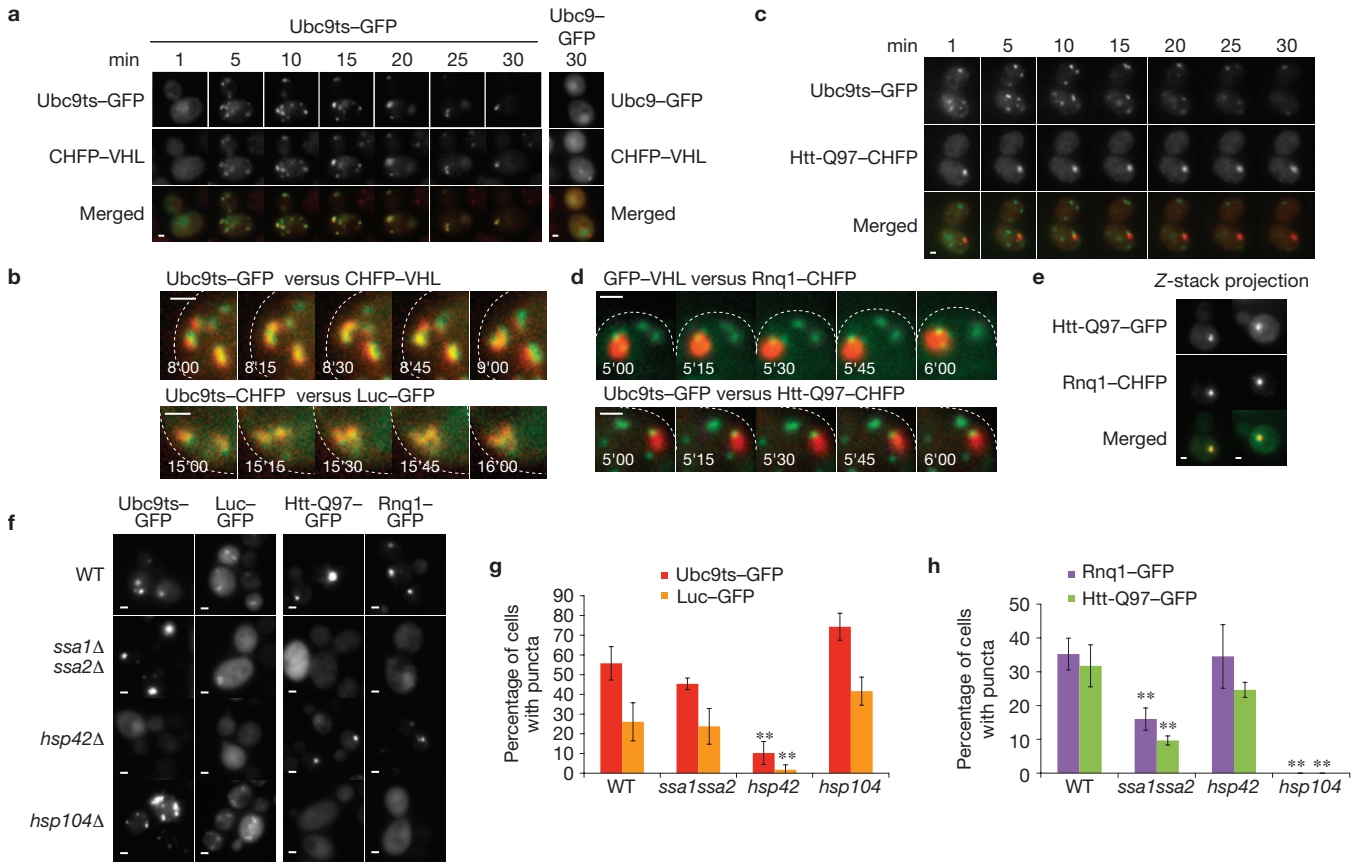

Figure 6 Different types of misfolded protein, but not amyloids, are processed together through the Q-body pathway. (**a**) WT cells expressing Ubc9ts–GFP and CHFP–VHL were grown at 28 °C in galactose medium and imaged at 37 °C in glucose medium. Five-minute series of images show Ubc9ts–GFP signal in green and CHFP–VHL signal in red. Cells expressing Ubc9–GFP and CHFP–VHL were similarly prepared and imaged 30 min after the shift. (**b**) 15-s-interval series of a cell represented in **a** (top panel) and from a cell co-expressing Luc–GFP and Ubc9–CHFP (bottom panel, and Supplementary Fig. S5a). (**c**) WT cells expressing Htt-Q97–CHFP (red) and Ubc9ts–GFP (green) were prepared and imaged as in **a**. (**d**) 15-s-interval series from a cell represented in **c** (bottom panel) and from a cell co-expressing GFP–VHL and Rnq1–CHFP (top panel, and Supplementary Fig. S5c). (**e**) Two-colour *Z*-stack projection of cells expressing both Htt-Q97–GFP (in green) and Rnq1–CHFP (in red). (**f**) GFP signal of WT, *ssa1*Δ*ssa2*Δ, *hsp42*Δ and *hsp104*Δ cells expressing Ubc9ts–GFP or Luc-GFP at 37 °C; or Htt-Q97–GFP or Rnq1–GFP at 28 °C. (**g**,**h**) Percentages of cells with puncta from a population analysed in **f**. Respective total population sizes for WT, *ssa1ssa2*, *hsp42* and *hsp104* cells: orange, $n = (2{,}418; 375; 3{,}013; 591)$ cells; yellow, $n = (1{,}035; 472; 442; 681)$ cells; purple, $n = (971; 519; 1{,}047; 617)$ cells; green, $n = (1{,}165; 410; 1{,}235; 853)$ cells, over three independent experiments (6 fields counted per experiment). The error bars represent mean and s.d. $^{**}P < 0.005$, compared with WT for the same indicated time. Scale bars: 1 μm.

The Q-body pathway is regulated by cellular status

Protein homeostasis is regulated by cellular status and is impaired during ageing, which may account for the late onset of many amyloid diseases[41–43]. We examined whether cellular state or ageing modulates the formation and processing of Q-bodies. Budding yeast enter a non-diving G0-like state when a culture is grown to stationary phase, a paradigm often referred to as chronological ageing[44]. Aged non-dividing cells expressing diffuse Ubc9ts–GFP were shifted to 37 °C and imaged. None of the aged cells was capable of inducing Q-bodies, unlike what is observed in young dividing cells (Fig. 7b and Supplementary Fig. S6). However, we did observe that aged cells contained pre-existing Hsp104-positive puncta as well as a distinct large inclusion containing Hsp42 (Fig. 7b), previously reported as a hallmark of chronologically aged cells[45].

The Q-body pathway is also regulated by TOR signalling, known to modulate protein homeostasis in response to nutrient and cellular state[42,46,47]. Treatment with 0.2 μg ml^{-1} rapamycin immediately before a 37 °C shift profoundly affected the Q-body pathway (Fig. 7c,d, and Supplementary Video S12) leading to rapid clearance of Q-bodies from the cytoplasm. Our data imply a regulatory role for TOR signalling in the Q-body pathway, and suggest that aged cells have lost their responsiveness to spatially sequester misfolded proteins.

Fitness advantage of chaperones providing spatial sequestration of misfolded proteins

Despite their role in Q-body formation and dissolution, Hsp42 and Hsp104 are dispensable both for misfolded protein degradation and growth at 37 °C (Supplementary Fig. S7). However, the existence of a general pathway for the active spatial sequestration of misfolded proteins argues for a potential benefit to the cells. We reasoned that sequestration into Q-bodies may purge the cellular milieu from potentially deleterious misfolded species, thereby providing a fitness advantage to cells during stress. To test this, we carried out competition experiments comparing the relative fitness of WT cells and cells lacking either Hsp42, Hsp26 or Hsp104 under normal and heat-stress conditions. Equal amounts of WT and mutant cells were mixed and

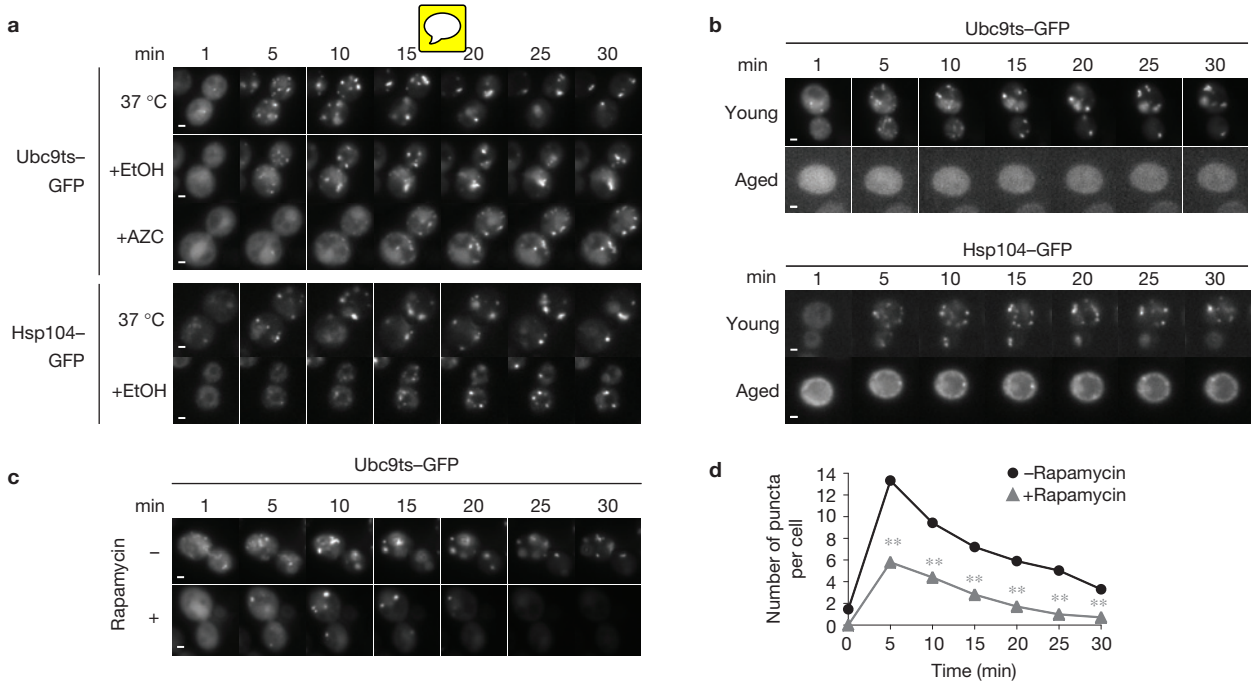

Figure 7 The Q-body pathway responds to proteotoxic stress, chronological ageing and nutrient signalling. (**a**) Ubc9ts–GFP-expressing cells were grown at 28 °C in galactose medium and Hsp104–GFP-expressing at 28 °C in glucose medium. Cells were imaged at 28 °C in glucose medium after a 10 min treatment with 10% ethanol (EtOH), 30 min treatment with 5 mg ml^{-1} AZC, or at 37 °C with no treatment. GFP signal is shown in 5 min series movies over 30 min. (**b**) Cells expressing Ubc9ts–GFP (top panel) or Hsp104–GFP (bottom panel) were grown at 28 °C for 5 h (young) or for 3 days (aged) and imaged at 37 °C. GFP signal is shown in 5 min series movies. (**c**) Ubc9ts–GFP-expressing cells were grown at 28 °C in galactose medium and imaged at 37 °C in glucose medium in the absence (–) or presence (+) of 0.2 μg ml^{-1} rapamycin 10 min before the shift. GFP signal is shown in 5 min series movies over 30 min. (**d**) Quantification of the average number of puncta per cell in untreated (–, circles) or rapamycin-treated (+, triangles) cells over time as presented in **c**. Puncta assessed from a total population of $n = 40$ cells over three independent experiment (3 fields counted per experiment). $^{**}P < 0.005$, compared with untreated cells for the same indicated time. Scale bars: 1 μm.

grown together at 28 °C or 37 °C, with daily dilutions, for 5 days. At each dilution, the proportion of WT and mutant cells was examined by comparing the number of kanamycin-resistant (KanR) colony-forming units (CFUs; mutant cells) versus kanamycin-sensitive CFUs (WT cells; Fig. 8a). Deletion of Hsp26 provides neither a fitness cost nor a benefit at either temperature. The equal proportion of WT and *hsp26*Δ cells was maintained throughout the 5 days of growth at either temperature (Fig. 8b), also indicating that KanR does not affect the fitness of mutant cells. Deletion of Hsp42 provided neither cost nor benefit at 28 °C (Fig. 8c, left panel). However, at 37 °C, deletion of Hsp42 was remarkably disadvantageous as WT cells outcompeted *hsp42*Δ cells after 2 days (Fig. 8c, right panel). Thus, Hsp42 provides a strong fitness advantage for cells subjected to stress. A parallel analysis for cells lacking Hsp104 proved surprising. Deletion of Hsp104 also reduced the fitness advantage of cells grown at 37 °C (Fig. 8d, right panel) suggesting that protein disaggregation is advantageous under conditions of stress. However, under normal growth conditions, that is, 28 °C, Hsp104 has a strong fitness cost, as *hsp104*Δ cells were much fitter than WT cells (Fig. 8d, left panel). As the main biochemical and cellular function of Hsp104 is to disaggregate misfolded and aggregated proteins, this suggests that a strong disaggregase activity is disadvantageous in the absence of stress-induced protein misfolding.

DISCUSSION

Misfolded protein clearance mechanisms were proposed to be hierarchical, whereby misfolded proteins are first stabilized by chaperones for either refolding or degradation with sequestration into inclusions as a second line of defence when proteostasis fails. Our study calls for a revision of this concept. We find that misfolded protein sequestration is a physiological and early response to the presence of misfolded proteins. Degradation occurs concurrently with Q-body processing, implying that sequestration is not necessarily a consequence of degradation failure. Q-bodies form in response to many stresses but become observable in larger inclusions upon proteostasis collapse, because their clearance is abrogated while their formation and coalescence continues. Compartmentalization into Q-bodies is not essential for degradation but may enhance cell fitness by sequestering potentially toxic misfolded species. Our findings provide a simple explanation to the genesis of large inclusions upon protein homeostasis dysfunction and UPS impairment that does not require invoking activation of special inclusion-formation mechanisms.

Misfolded protein concentration into Q-bodies is an active process that requires molecular chaperones. The Hsp70–Hsp90–Hsp110 system, which also participates in the degradation and refolding of misfolded proteins[48,49], is central to the formation and dynamics of Q-bodies. These chaperones probably constitute the core of the cytoplasmic quality control system. Q-bodies are associated with the ER, which may provide a basis for Q-body movement and coalescence through its tubular and dynamic network throughout the cytosol. ER-associated J-domain proteins, Ydj1 and Hlj1 (refs 29,32), are important for Q-body concentration and maturation, consistent with their role recruiting Ssa1 to the ER membrane[32,50]. However,

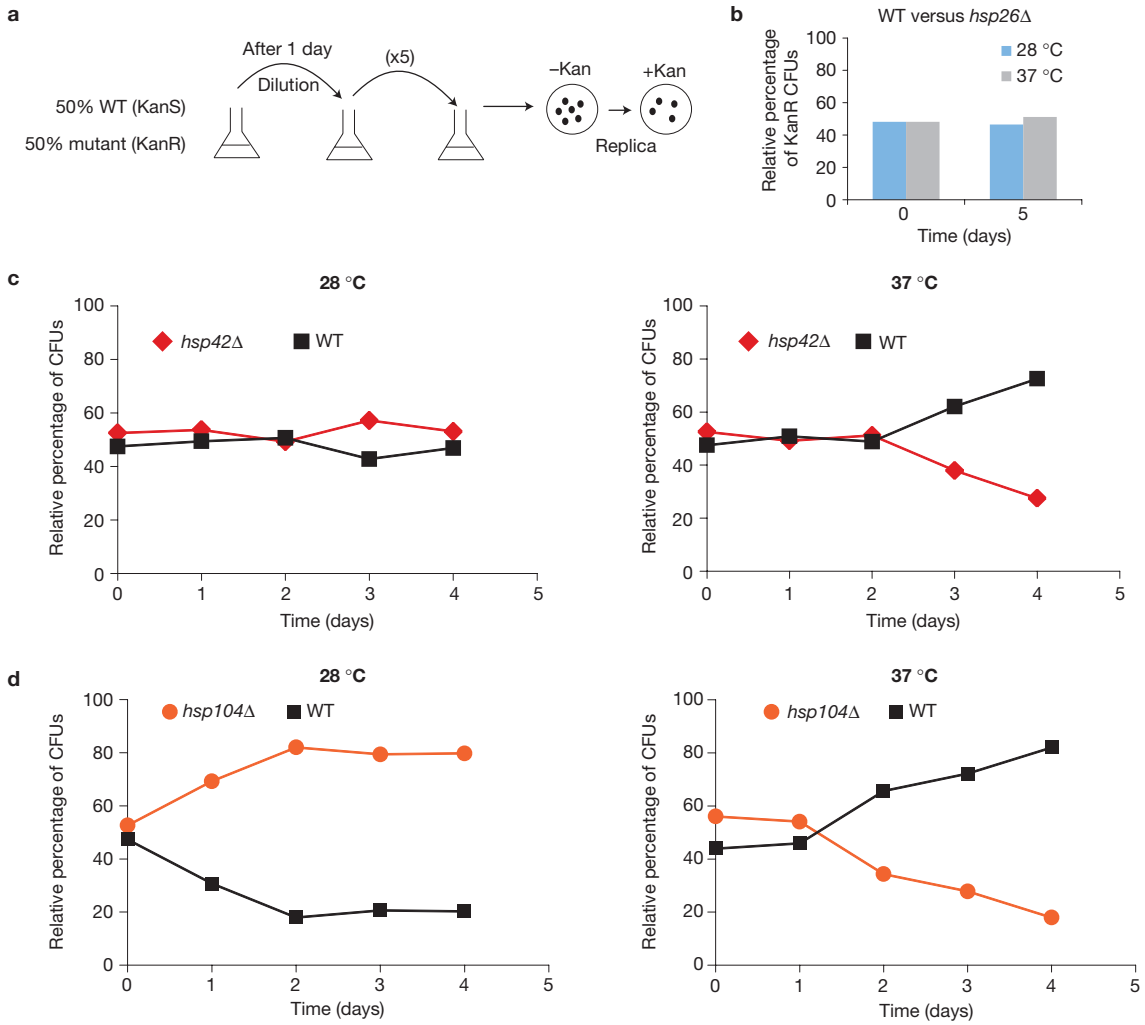

Figure 8 Fitness advantage of spatial sequestration of misfolded proteins in Q-bodies. (**a**) Schematic of competition assay. KanS, kanamycin-sensitive phenotype; KanR, kanamycin-resistant phenotype. (**b**) Percentage of KanR *hsp26*Δ CFUs over KanS WT CFUs was quantified at 0 and 5 days. (**c**,**d**) Percentage of KanR *hsp42*Δ CFUs (**c**) or *hsp104*Δ CFUs (**d**) over KanS WT CFUs was quantified over time at 28 °C (left panels) or 37 °C (right panels). Data represent three independent experiments ($n = 350$ CFUs for each day of the experiment).

their function is not essential, probably owing to functional overlaps between J-domain proteins[31].

The small HSP Hsp42 and the disaggregase Hsp104 contribute to Q-body dynamics. Epistasis analyses of mutations in Hsp42, Hsp104 and Sse1 suggest that at least part of Q-body dynamics results from the balance between addition and dissolution activities. A simple model explaining our data is that puncta formation involves the action of different chaperones, notably Hsp42 and J-domain proteins, whereas Q-body growth occurs at the expense of Hsp104- or Sse1-mediated dissolution of others. Interestingly, a similar cycle of addition–dissolution is proposed to govern P-granule dynamics and the asymmetric partition of maternally inherited messenger RNAs (ref. 51). However, coalescence may also involve direct merging of Q-bodies with the help of chaperones and additional factors.

Q-body formation, dynamics and clearance are independent of either actin or tubulin cytoskeleton, consistent with previous analysis of the dynamics of Hsp104-associated proteins aggregates[52] and in contrast to alternative proposals[7,14]. Importantly, our finding that prolonged depolymerization of the actin cytoskeleton has deleterious effects on the Q-body pathway suggests an explanation to reconcile these discrepancies. Unassembled actin may bind to and titrate quality control components, generally impairing cellular proteostasis. The cytoskeleton may also be required for asymmetric partitioning of inclusions, a question that is not addressed here. Future studies incorporating our findings should illuminate the link between the cytoskeleton, protein homeostasis and the inheritance of misfolded protein inclusions.

Without proteasome inhibition, misfolded proteins are not directly targeted to a static pre-existing quality control compartment, but concentrated throughout the cell in multiple dynamic Q-bodies. The link between Q-bodies and compartments previously observed in the presence of proteasome inhibition[6–8,14] remains to be determined. These structures may be end points of the Q-body pathway resulting from the coalescence of Q-bodies when clearance is impaired. The observation that some perinuclear puncta lack Hsp104 can explain the appearance of the JUNQ upon proteasome inhibition; puncta with slower dissolution rates would eventually grow at the expense of those with higher Hsp104 levels and faster disaggregation kinetics. It will be interesting to determine whether proteasome inhibition alters

the composition and properties of these structures, for instance by stabilizing labile quality control factors as suggested in ref. 8.

Amyloidogenic proteins sequestered in the insoluble IPOD seem to bypass the Q-body pathway. Perhaps IPOD substrates interact aberrantly with chaperones that recruit substrates to the Q-body pathway thereby failing to be cleared. Alternatively, dense amyloid structures may be more refractory to disaggregation, thereby eluding the Q-body cycle. Interestingly, Q-body dynamics is impaired in the presence of an IPOD, suggesting that the IPOD alters cellular proteostasis. Several studies reported that amyloid inclusions sequester chaperones, causing aggregation of unrelated proteins without their co-aggregation with the amyloid inclusion[53,54]. The impairment of the Q-body pathway during ageing could render aged cells more sensitive to stress and misfolding, consistent with their enhanced sensitivity to protein misfolding[55]. Understanding the regulation of the Q-body pathway and its relation to other reported quality control structures may provide new therapeutical targets for conformational disorders, including Alzheimer's and Huntington's disease.

Our data raise the question of what the function of Q-bodies is. Sequestering misfolded proteins is dispensable for degradation but may help clear the cytosol of potentially toxic misfolded species, store labile proteins for later use and/or facilitate quality control by concentrating chaperones and substrates on a two-dimensional surface. Loss of chaperones involved in Q-body formation and dynamics leads to a fitness reduction in stressed cells. Surprisingly, the robust disaggregase Hsp104 is deleterious under normal growth conditions. This could explain the long-standing enigma of why Hsp104 is found only in yeast, plants and bacteria, generally subjected to repeated and severe stress[56], but not in metazoan cells, which control their stress responses through organism-wide cell non-autonomous circuits[57,58]. For these multicellular organisms, the advantage provided by Hsp104 during stress may not compensate for the disadvantage of having a potent cellular disaggregase under normal conditions. These results highlight the delicate tuning of quality control pathways during evolution.

Concentration of misfolded proteins in Q-bodies creates a dynamic and flexible management system conferring fitness pending the impact of the immediate environmental changes challenging the cell. The relationship between the biochemical functions of chaperones and their spatial organization within the cell will be instrumental to understand folding impairments during pathological states. □

METHODS

Methods and any associated references are available in the online version of the paper.

Note: Supplementary Information is available in the online version of the paper

ACKNOWLEDGEMENTS

We thank C. Toret and V. Albanese for experimental advice and discussions; and C. Toret and R. Andino for critical reading of the manuscript. S.E-T. was initially supported by a fellowship from Fondation pour la Recherche Medicale (France). W.I.M.V. was supported by the Marie Curie International Outgoing Fellowship Programme. This work was supported by grants from the NIH and a Senior Scholar Award from the Ellison Foundation to J.F.

AUTHOR CONTRIBUTIONS

S.E-T. and J.F. conceived the project, S.E-T. performed most experiments, W.I.M.V. performed experiments in Fig. 1d,e, Fig. 3e,f and Supplementary Fig. S1b, and all authors interpreted the experiments and contributed to writing.

COMPETING FINANCIAL INTERESTS

The authors declare no competing financial interests.

Published online at www.nature.com/doifinder/10.1038/ncb2838
Reprints and permissions information is available online at www.nature.com/reprints

1. Balch, W. E., Morimoto, R. I., Dillin, A. & Kelly, J. W. Adapting proteostasis for disease intervention. *Science* **319,** 916–919 (2008).
2. Lindquist, S. L. & Kelly, J. W. Chemical and biological approaches for adapting proteostasis to ameliorate protein misfolding and aggregation diseases: progress and prognosis. *Cold Spring Harb. Perspect. Biol.* **3,** 1–34 (2011).
3. Chiti, F. & Dobson, C. M. Protein misfolding, functional amyloid, and human disease. *Ann. Rev. Biochem.* **75,** 333–366 (2006).
4. Houck, S.A., Singh, S. & Cyr, D. M. Cellular responses to misfolded proteins and protein aggregates. *Methods Mol. Biol.* **832,** 455–461 (2012).
5. Chen, B., Retzlaff, M., Roos, T. & Frydman, J. Cellular strategies of protein quality control. *Cold Spring Harb. Perspect. Biol.* **3,** a004374 (2011).
6. Kaganovich, D., Kopito, R. & Frydman, J. Misfolded proteins partition between two distinct quality control compartments. *Nature* **454,** 1088–1095 (2008).
7. Specht, S., Miller, S. B., Mogk, A. & Bukau, B. Hsp42 is required for sequestration of protein aggregates into deposition sites in *Saccharomyces cerevisiae*. *J. Cell Biol.* **195,** 617–629 (2011).
8. Malinovska, L., Kroschwald, S., Munder, M. C., Richter, D. & Alberti, S. Molecular chaperones and stress-inducible protein-sorting factors coordinate the spatiotemporal distribution of protein aggregates. *Mol. Biol. Cell* **23,** 3041–3056 (2012).
9. Johnston, J. A., Ward, C. L. & Kopito, R. R. Aggresomes: a cellular response to misfolded proteins. *J. Cell Biol.* **143,** 1883–1898 (1998).
10. Zhang, X. & Qian, S. B. Chaperone-mediated hierarchical control in targeting misfolded proteins to aggresomes. *Mol. Biol. Cell* **22,** 3277–3288 (2011).
11. Douglas, P. M., Summers, D. W. & Cyr, D. M. Molecular chaperones antagonize proteotoxicity by differentially modulating protein aggregation pathways. *Prion* **3,** 51–58 (2009).
12. Cohen, E., Bieschke, J., Perciavalle, R. M., Kelly, J. W. & Dillin, A. Opposing activities protect against age-onset proteotoxicity. *Science* **313,** 1604–1610 (2006).
13. Arrasate, M., Mitra, S., Schweitzer, E. S., Segal, M. R. & Finkbeiner, S. Inclusion body formation reduces levels of mutant huntingtin and the risk of neuronal death. *Nature* **431,** 805–810 (2004).
14. Liu, B. *et al.* The polarisome is required for segregation and retrograde transport of protein aggregates. *Cell* **140,** 257–267 (2010).
15. Nakatogawa, H., Ichimura, Y. & Ohsumi, Y. Atg8, a ubiquitin-like protein required for autophagosome formation, mediates membrane tethering and hemifusion. *Cell* **130,** 165–178 (2007).
16. Sheth, U. & Parker, R. Targeting of aberrant mRNAs to cytoplasmic processing bodies. *Cell* **125,** 1095–1109 (2006).
17. Toshima, J. Y. *et al.* Spatial dynamics of receptor-mediated endocytic trafficking in budding yeast revealed by using fluorescent alpha-factor derivatives. *Proc. Natl Acad. Sci. USA* **103,** 5793–5798 (2006).
18. Wright, R., Basson, M., D'Ari, L. & Rine, J. Increased amounts of HMG-CoA reductase induce "karmellae": a proliferation of stacked membrane pairs surrounding the yeast nucleus. *J. Cell Biol.* **107,** 101–114 (1988).
19. Shibata, Y., Voeltz, G. K. & Rapoport, T. A. Rough sheets and smooth tubules. *Cell* **126,** 435–439 (2006).
20. Voeltz, G. K., Prinz, W. A., Shibata, Y., Rist, J. M. & Rapoport, T. A. A class of membrane proteins shaping the tubular endoplasmic reticulum. *Cell* **124,** 573–586 (2006).
21. Shibata, Y. *et al.* The reticulon and DP1/Yop1p proteins form immobile oligomers in the tubular endoplasmic reticulum. *J. Biol. Chem.* **283,** 18892–18904 (2008).
22. West, M., Zurek, N., Hoenger, A. & Voeltz, G. K. A 3D analysis of yeast ER structure reveals how ER domains are organized by membrane curvature. *J. Cell Biol.* **193,** 333–346 (2011).
23. McDonough, H. & Patterson, C. CHIP: a link between the chaperone and proteasome systems. *Cell Stress Chaperones* **8,** 303–308 (2003).
24. Mayer, M. P. & Bukau, B. Hsp70 chaperones: cellular functions and molecular mechanism. *Cell Mol. Life Sci.* **62,** 670–684 (2005).
25. McClellan, A. J., Scott, M. D. & Frydman, J. Folding and quality control of the VHL tumor suppressor proceed through distinct chaperone pathways. *Cell* **121,** 739–748 (2005).
26. Coppinger, J. A. *et al.* A chaperone trap contributes to the onset of cystic fibrosis. *PLoS One* **7,** e37682 (2012).
27. Schneider, C. *et al.* Pharmacologic shifting of a balance between protein refolding and degradation mediated by Hsp90. *Proc. Natl Acad. Sci. USA* **93,** 14536–14541 (1996).
28. Becker, J., Walter, W., Yan, W. & Craig, E. A. Functional interaction of cytosolic hsp70 and a DnaJ-related protein, Ydj1p, in protein translocation *in vivo*. *Mol. Cell Biol.* **16,** 4378–4386 (1996).
29. Caplan, A. J., Tsai, J., Casey, P. J. & Douglas, M. G. Farnesylation of YDJ1p is required for function at elevated growth temperatures in *Saccharomyces cerevisiae*. *J. Biol. Chem.* **267,** 18890–18895 (1992).

30. Flom, G. A., Lemieszek, M., Fortunato, E. A. & Johnson, J. L. Farnesylation of Ydj1 is required for *in vivo* interaction with Hsp90 client proteins. *Mol. Biol. Cell* **19,** 5249–5258 (2008).
31. Kampinga, H. H. & Craig, E. A. The HSP70 chaperone machinery: J proteins as drivers of functional specificity. *Nat. Rev. Mol. Cell Biol.* **11,** 579–592 (2010).
32. Youker, R. T., Walsh, P., Beilharz, T., Lithgow, T. & Brodsky, J. L. Distinct roles for the Hsp40 and Hsp90 molecular chaperones during cystic fibrosis transmembrane conductance regulator degradation in yeast. *Mol. Biol. Cell* **15,** 4787–4797 (2004).
33. Shorter, J. & Lindquist, S. Hsp104, Hsp70 and Hsp40 interplay regulates formation, growth and elimination of Sup35 prions. *EMBO J.* **27,** 2712–2724 (2008).
34. Tipton, K. A., Verges, K. J. & Weissman, J. S. *In vivo* monitoring of the prion replication cycle reveals a critical role for Sis1 in delivering substrates to Hsp104. *Mol. Cell* **32,** 584–591 (2008).
35. Gupta, R. *et al.* Firefly luciferase mutants as sensors of proteome stress. *Nat. Methods* **8,** 879–884 (2011).
36. Chernoff, Y. O., Lindquist, S. L., Ono, B., Inge-Vechtomov, S. G. & Liebman, S. W. Role of the chaperone protein Hsp104 in propagation of the yeast prion-like factor [psi +]. *Science* **268,** 880–884 (1995).
37. Sondheimer, N. & Lindquist, S. Rnq1: an epigenetic modifier of protein function in yeast. *Mol. Cell* **5,** 163–172 (2000).
38. Meriin, A. B. *et al.* Huntington toxicity in yeast model depends on polyglutamine aggregation mediated by a prion-like protein Rnq1. *J. Cell Biol.* **157,** 997–1004 (2002).
39. Piper, P. W. The heat shock and ethanol stress responses of yeast exhibit extensive similarity and functional overlap. *FEMS Microbiol. Lett.* **134,** 121–127 (1995).
40. Trotter, E. W. *et al.* Misfolded proteins are competent to mediate a subset of the responses to heat shock in *Saccharomyces cerevisiae*. *J. Biol. Chem.* **277,** 44817–44825 (2002).
41. Morimoto, R. I. Proteotoxic stress and inducible chaperone networks in neurodegenerative disease and aging. *Genes Dev.* **22,** 1427–1438 (2008).
42. Conn, C. S. & Qian, S. B. mTOR signaling in protein homeostasis: less is more? *Cell Cycle* **10,** 1940–1947 (2011).
43. Taylor, R. C. & Dillin, A. Aging as an event of proteostasis collapse. *Cold Spring Harb. Perspect. Biol.* **3,** 1–17 (2011).
44. Fabrizio, P. & Longo, V. D. The chronological life span of *Saccharomyces cerevisiae*. *Aging Cell* **2,** 73–81 (2003).
45. Narayanaswamy, R. *et al.* Widespread reorganization of metabolic enzymes into reversible assemblies upon nutrient starvation. *Proc. Natl Acad. Sci. USA* **106,** 10147–10152 (2009).
46. Peters, T. W. *et al.* Tor1 regulates protein solubility in *Saccharomyces cerevisiae*. *Mol. Biol. Cell* **23,** 4679–4688 (2012).
47. Kapahi, P. *et al.* With TOR, less is more: a key role for the conserved nutrient-sensing TOR pathway in aging. *Cell Metab.* **11,** 453–465 (2010).
48. Glover, J. R. & Lindquist, S. Hsp104, Hsp70, and Hsp40: a novel chaperone system that rescues previously aggregated proteins. *Cell* **94,** 73–82 (1998).
49. Mandal, A. K. *et al.* Hsp110 chaperones control client fate determination in the hsp70-Hsp90 chaperone system. *Mol. Biol. Cell* **21,** 1439–1448 (2010).
50. Huyer, G. *et al.* Distinct machinery is required in *Saccharomyces cerevisiae* for the endoplasmic reticulum-associated degradation of a multispanning membrane protein and a soluble luminal protein. *J. Biol. Chem.* **279,** 38369–38378 (2004).
51. Ouellet, J. & Barral, Y. Organelle segregation during mitosis: lessons from asymmetrically dividing cells. *J. Cell Biol.* **196,** 305–313 (2012).
52. Zhou, C. *et al.* Motility and segregation of Hsp104-associated protein aggregates in budding yeast. *Cell* **147,** 1186–1196 (2011).
53. Gidalevitz, T., Krupinski, T., Garcia, S. & Morimoto, R. I. Destabilizing protein polymorphisms in the genetic background direct phenotypic expression of mutant SOD1 toxicity. *PLoS Genet.* **5,** e1000399 (2009).
54. Olzscha, H. *et al.* Amyloid-like aggregates sequester numerous metastable proteins with essential cellular functions. *Cell* **144,** 67–78 (2011).
55. Kikis, E. A., Gidalevitz, T. & Morimoto, R. I. Protein homeostasis in models of aging and age-related conformational disease. *Adv. Exp. Med. Biol.* **694,** 138–159 (2010).
56. Shorter, J. Hsp104: a weapon to combat diverse neurodegenerative disorders. *Neurosignals* **16,** 63–74 (2008).
57. Gidalevitz, T., Prahlad, V. & Morimoto, R. I. The stress of protein misfolding: from single cells to multicellular organisms. *Cold Spring Harb. Perspect. Biol.* **3,** 1–18 (2011).
58. Durieux, J., Wolff, S. & Dillin, A. The cell-non-autonomous nature of electron transport chain-mediated longevity. *Cell* **144,** 79–91 (2011).

DOI: 10.1038/ncb2838

METHODS

Yeasts, plasmids and media. All yeast deletion strains used in this study derived from BY4741 or BY4742 wild-type (WT) strains, obtained from the *Saccharomyces* Genome Deletion Project[59], except for *HSP82* [*hsc82 Δ::LEU2 hsp82Δ::LEU2 his3-11,15::GPD-HSP82(HIS3) can1-100 ade2-1 his3-11,15 leu2-3,12 trp1-1 ura3-1*]; *hsp82ts* [*hsc82Δ::LEU2 hsp82Δ::LEU2 his3-11,15::GPD-hsp82(G170D) (HIS3) can1-100 ade2-1 his3-11,15 leu2-3,12 trp1-1 ura3-1*] (ref. 60); *hlj1*Δ[*MAT**a**, ade2, his3, leu2, ura3, trp1, Δhlj1::HIS3*]; *hlj1Δydj1-151*[*MATα, ade2, his3, leu2, ura3, trp1, can1-100 ydj1-2::HIS3, ydj1-151::LEU2, hlj1::TRP1*] (ref. 32); and *ssa1ts ssa2Δssa3Δssa4Δ*[*MATα leu2-3,112 his3-11 ura3-52 trp1Δ1 lys2 ssa1-45: URA3 ssa2::LEU2 ssa3::TRP1 ssa4::LYS2*] (ref. 28).

We acknowledge the generous gifts of the Abp1–GFP strain (D. Drubin, University of California Berkeley, California, USA)[61], *rtn1Δrtn2Δyop1* (T. Rapoport, Harvard Medical School, Massachusetts, USA)[20]; *hlj1Δ* and *hlj1Δydj1-151* (J. Brodsky, University of Pittsburgh, Philadelphia, USA)[32].

Double-mutant strains were obtained by mating and sporulation, or by transformation with a deletion cassette[62,63].

The plasmids carrying the GFP-tagged fusions were constructed as followed. Ubc9ts (Ubc9-2), VHL, Rnq1, Htt-Q97 and luciferase were cloned using the Gateway cloning technology into pAG416Gal1–ccdB–GFP, pAG413Gal1–ccdB–GFP, pAG416Gal1–GFP–ccdB or pAG413Gal1–ccdB–GFP Gateway destination vectors[64]. The Cherry fusion plasmids were obtained in 2 steps. First, the Cherry (CHFP) gene was cloned into the pAG416Gal1–ccdB Gateway plasmid using HindIII and XhoI, and second the gene of interest was transferred into the resulting plasmid using the Gateway technology. CHFP–Atg8 was previously described[6]. GFP–Snc1 (pKT1490) and GFP–Pep12 (pKT1487) plasmids were generously provided by K. Tanaka[65]. Of note, the GFP-tagged chaperones used in this study were functional by different assays.

Cells were grown in rich media YPD or YPGal (2% galactose) or in glucose or galactose synthetic minimum media.

Gal shut-off assay. Cells were grown overnight in raffinose synthetic media at 28 °C before dilution to an attenuance (D) of 0.1–0.3 at 600 nm in galactose synthetic media. The cells were grown for 4–6 h at 28 °C to induce the expression of the galactose-inducible gene of interest. A first sample of an equivalent of 10 D units was collected ($t = 0$) and the rest of the culture was simultaneously shifted to 37 °C and in glucose synthetic media to specifically shut-off the expression of the gal-inducible promoter. Typically, the same amount of cells was collected at 15, 30 and 60 min after the shift. The samples were centrifuged, washed once in water, and the pellet was frozen in liquid nitrogen. The extraction of protein was carried out using a 6 M urea buffer (50 mM Tris–HCl at pH 7.5, 0.5% SDS and 6 M urea) supplemented with 1 mM dithiothreitol, 1 mM phenylmethylsulphonyl fluoride and protease inhibitor cocktail. Cells were broken by glass beads and centrifuged for 2 min at 2,000g. Supernatant protein concentration was quantified by a BCA protein assay kit (Pierce) and equivalents of 50 µg of proteins were loaded on SDS–PAGE. Proteins were transferred onto a nitrocellulose membrane and immunoblotted with primary antibodies against GFP (1:10,000, Roche, catalogue number 11814460001) or actin (1:10,000, Sigma, catalogue number A5441). Secondary antibodies used were goat-anti-mouse IRDye 680LT (1:15,000; LI-COR Biosciences, catalogue number 926-68020). Membranes were scanned using an Odyssey imager and software (LI-COR Biosciences).

Fluorescence microscopy. Standard microscopy. As in the gal shut-off assay, cells were grown overnight in raffinose media followed by 4–6 h at 28 °C in galactose media to induce the expression. Then, the cells were heat-shocked at 37 °C in glucose media for 30 min or 1 h before being mounted on glass slides. Alternatively, cells were shifted to 37 °C and kept in galactose media for steady-state analyses. Fluorescence was visualized using a Zeiss Axiovert 200 inverted microscope equipped with FITC/rhodamine/Cy5 filter sets (Chroma), a ×100 NA 1.3 oil-immersion objective (Olympus) and a digital Axiocam MRm camera (Carl Zeiss) controlled with Axiovison software. Image analyses was performed by ImageJ software (http://rsbweb.nih.gov/ij).

Live-cell imaging. Cells were grown in raffinose and galactose at 28 °C, as described for standard fluorescence. Cells were then immobilized on concanavalin A-coated coverslips. Samples were washed in glucose media and kept in the same medium by sealing the coverslips to slides with vacuum grease. When indicated, cells were treated 10 min before sealing with 100 µM MG132 (Cayman Chemical), 200 µM of latrunculin A (Sigma), 15 µg ml^{-1} of nocodazole (Sigma), 10% ethanol, 5 mg ml^{-1} azetidine 2-carboxylic acid (AZC; Sigma) or 0.2 µg ml^{-1} rapamycin; alternatively, cells were treated for 30 min with 10 mM sodium azide and 10 mM deoxyglycose (Sigma) or 10 µM MDY64 (Invitrogen) before sealing. Imaging was done at 37 °C (or room temperature (25 °C) when indicated) using a Zeiss Axiovert 200M inverted microscope customized by Intelligent Imaging. Epifluorescence was provided by a Xenon lamp (DG4300W; Sutter Instrument) and visualized using Cy5/Cy3/FITC filter set and a ×100 NA 1.4 oil objective (Olympus). Images were acquired with a HQ CoolSNAP camera (Roper Scientific), and the system was controlled with Slidebook software. Movies were analysed with ImageJ software and only defined bright puncta were counted.

Deconvolution microscopy. Cells were grown in raffinose and galactose at 28 °C, and mounted on a slide as indicated for the live-cell imaging. Slides were incubated for 10 min at 37 °C and visualized using an IX70 Olympus inverted microscope equipped with a ×60 NA 1.4 oil objective; 490/20 (FITC/GFP) and 555/28 (Rhodamine, Cy3) excitation filters; 528/38 (FITC, GFP) and 617/73 (Rhodamine, Cy3) emission filters; and a HQ CoolSNAP camera (Princeton). Raw data were deconvolved using SoftWoRx software that controlled the system and images were analysed using ImageJ software.

Statistical analysis. Blinded puncta counting was used to assess the number of puncta in each cell. Statistical analysis was performed using Student's t-test with a two-tailed distribution.

Competition assay. WT and mutant cells were each grown in YPD medium. Equal numbers of cells from each culture were mixed in fresh YPD medium and diluted to $D_{600\,nm}$ 0.05 each (0.1 final). At 24 h intervals, the culture was diluted to $D = 0.1$ in YPD over 5 days. Each day, at the time of the dilution, an aliquot of the culture was plated at ∼200 colonies per YPD plate. Plates were replica plated on YPD with or without 50 µg ml^{-1} kanamycin. The ratio of kanamycin-resistant to kanamycin-sensitive colonies was recorded.

Dilution plating. Cells were suspended in water to a final $D_{600\,nm} \sim 1$ and tenfold serially diluted for subsequent spotting onto plates. Ten microlitres of each dilution sample was spotted onto YPD plates and grown at 28 °C or 37 °C.

Ageing assay. Cells were grown overnight in YPD at 28 °C and diluted to $D_{600\,nm} = 0.1$ in YPGal medium when they expressed Ubc9ts–GFP or in YPD medium when they expressed Hsp104–GFP or Hsp42–GFP. Cells were grown for either 4 h (young) or 3 days (aged) at 28 °C before being live-cell imaged. Samples were prepared as previously described except that cells were imaged in PBS buffer instead of medium.

59. Winzeler, E. A. *et al.* Functional characterization of the *S. cerevisiae* genome by gene deletion and parallel analysis. *Science* **285,** 901–906 (1999).
60. Nathan, D. F. & Lindquist, S. Mutational analysis of Hsp90 function: interactions with a steroid receptor and a protein kinase. *Mol. Cell Biol.* **15,** 3917–3925 (1995).
61. Kaksonen, M., Toret, C. P. & Drubin, D. G. A modular design for the clathrin- and actin-mediated endocytosis machinery. *Cell* **123,** 305–320 (2005).
62. Longtine, M. S. *et al.* Additional modules for versatile and economical PCR-based gene deletion and modification in *Saccharomyces cerevisiae*. *Yeast* **14,** 953–961 (1998).
63. Janke, C. *et al.* A versatile toolbox for PCR-based tagging of yeast genes: new fluorescent proteins, more markers and promoter substitution cassettes. *Yeast* **21,** 947–962 (2004).
64. Alberti, S., Gitler, A. D. & Lindquist, S. A suite of Gateway cloning vectors for high-throughput genetic analysis in *Saccharomyces cerevisiae*. *Yeast* **24,** 913–919 (2007).
65. Furuta, N., Fujimura-Kamada, K., Saito, K., Yamamoto, T. & Tanaka, K. Endocytic recycling in yeast is regulated by putative phospholipid translocases and the Ypt31p/32p-Rcy1p pathway. *Mol. Biol. Cell* **18,** 295–312 (2007).

DOI: 10.1038/ncb2838

nature cell biology

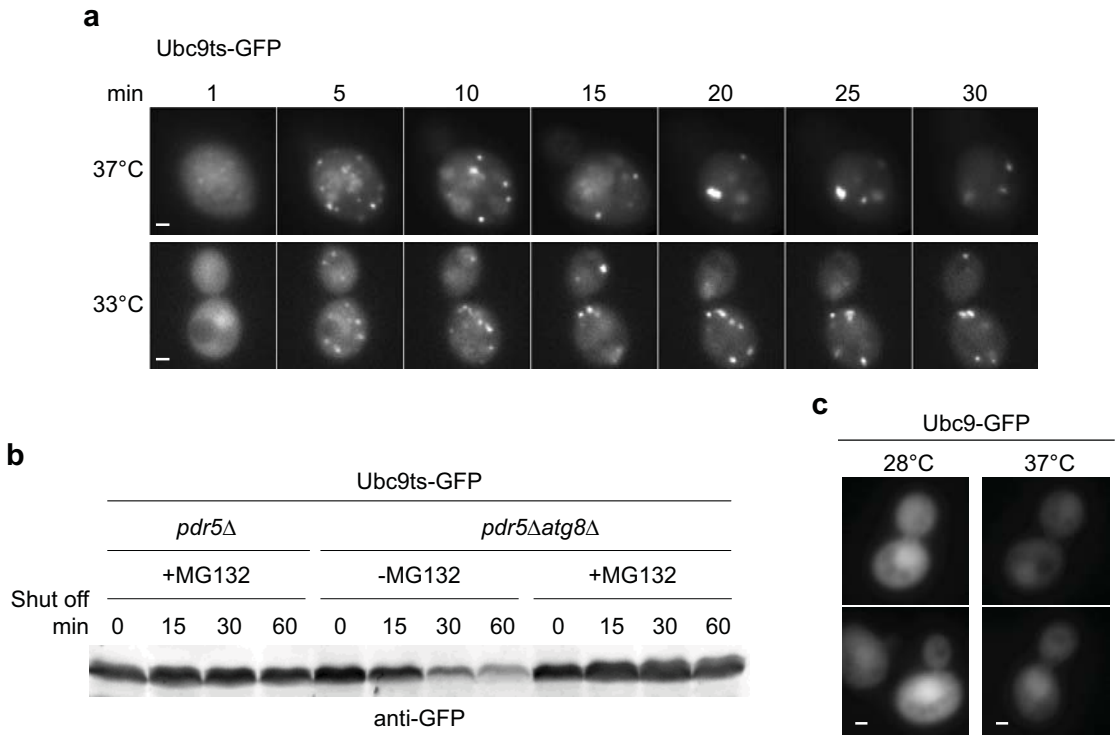

Figure S1 Formation of Q-bodies. (**a**) WT cells expressing Ubc9ts-GFP were grown at 28°C in galactose medium and shifted at 33°C or 37°C in glucose medium. 5 min series images shows Ubc9ts-GFP signal over a 30 min movie. Scale bars equal 1 µm. (**b**) *pdr5Δ* and *pdr5Δatg8Δ* cells expressing Ubc9ts-GFP were grown as in **a.** Upon temperature shift, cells were treated with 100 µM MG132 as indicated. Ubc9ts-GFP was analyzed by immunoblot using anti-GFP antibodies. (**c**) Images of Ubc9-GFP expressed in WT cells at 28°C (left panel) and shifted for 15 min at 37°C. GFP (right panel). Scale bars equal 1.5 µm.

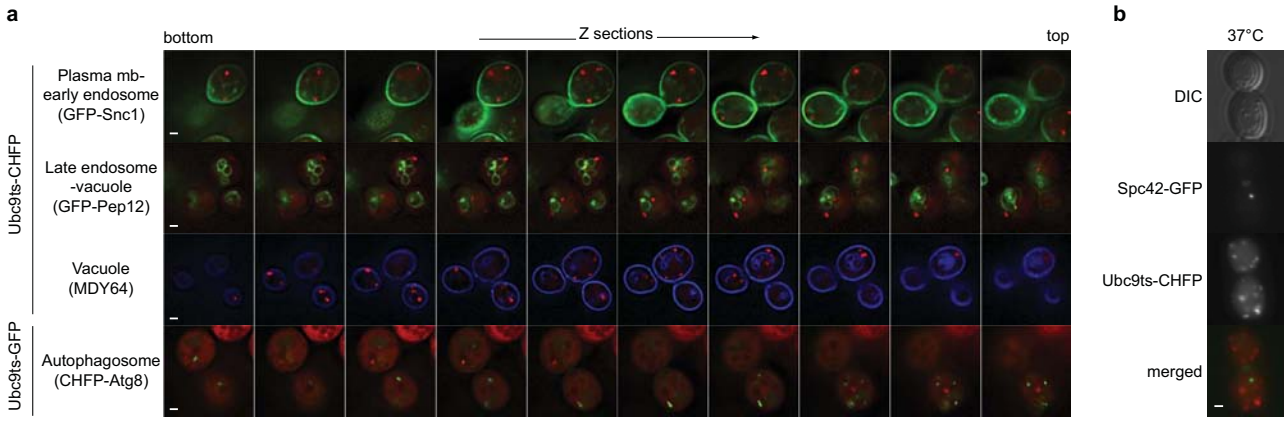

Figure S2 Q-bodies associate with specific sub-cellular structures. (**a**) Two-color images of Z-focal plans (0.2 μm intervals; obtained after 10 min at 37°C) of cells expressing Ubc9ts-CHFP (red) or Ubc9ts-GFP (green) and the following markers: GFP-Snc1 (early endosomes; green), GFP-Pep12 (late endosomes; green), CHFP-Atg8 (autophagic vesicles; red); the vacuole was imaged by treating cells with MDY64 (blue). Scale bars equal 1 μm.(**b**) Cells expressing Spc42-GFP (green) and Ubc9ts-CHFP (red) were imaged 15 min after a shift from 28°C to 37°C. Scale bars equal 1 μm.

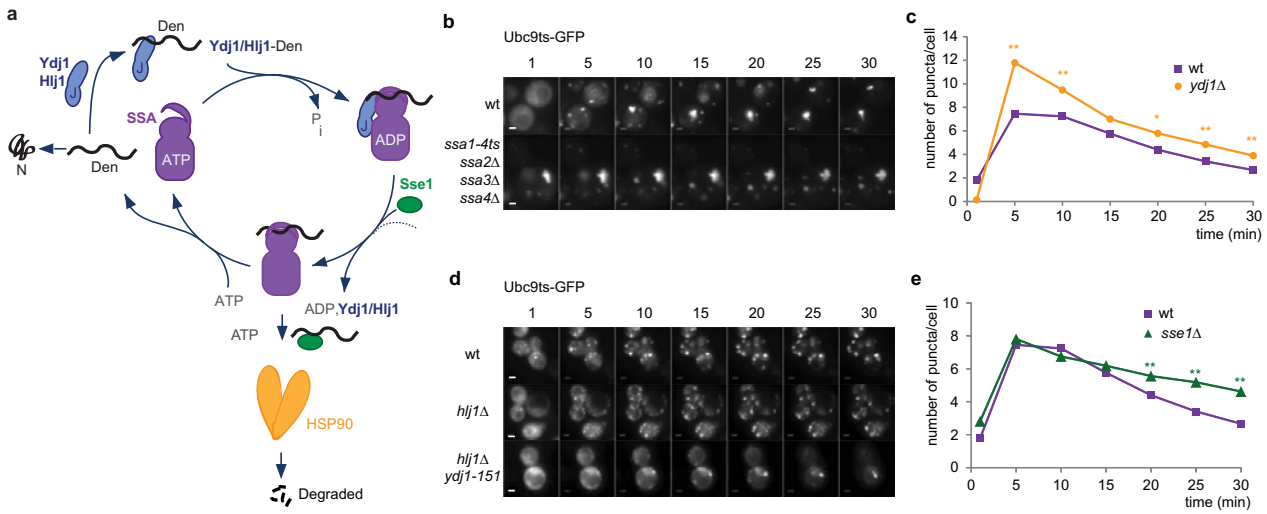

Figure S3 Hsp70-Hsp90 chaperones promote the maturation and degradation of Q-bodies. (**a**) Schematic of the Hsp70 chaperone system and its connection to the Hsp90 system. (**b**) Ubc9ts-GFP was expressed in WT and *ssa1-4 ssa2*D*ssa3*D*ssa4*Δ (herein *ssa1ts ssa2*D*ssa3*D*ssa4*Δ) background at 28°C in galactose medium and shifted at 37°C in glucose medium. 5 min series of images shows Ubc9ts-GFP in these strains over 30 min. Scale bars equal 1 µm. (**c**) Representation of the average number of puncta per cell in the WT (purple squares) and the *ydj1*Δ (orange circles) strains over time. Puncta assessed from a total population of n=38 cells over three independent experiments (1 field counted per experiment). (*) $p < 0.05$ (**) $p < 0.005$ compared to WT for the same indicated time.(**d**) Ubc9ts-GFP expressed in WT, *hlj1*Δ and *hlj1*D*ydj1-151* cells was imaged as in **b**. Scale bar equals 1 µm. (**e**) Average number of puncta per cell in the WT (purple squares) and the *sse1*Δ (green triangles) strains over timePuncta assessed from a total population of n=16 cells over three independent experiments (1 field counted per experiment). (**) $p < 0.005$ compared to the WT for the same indicated time.

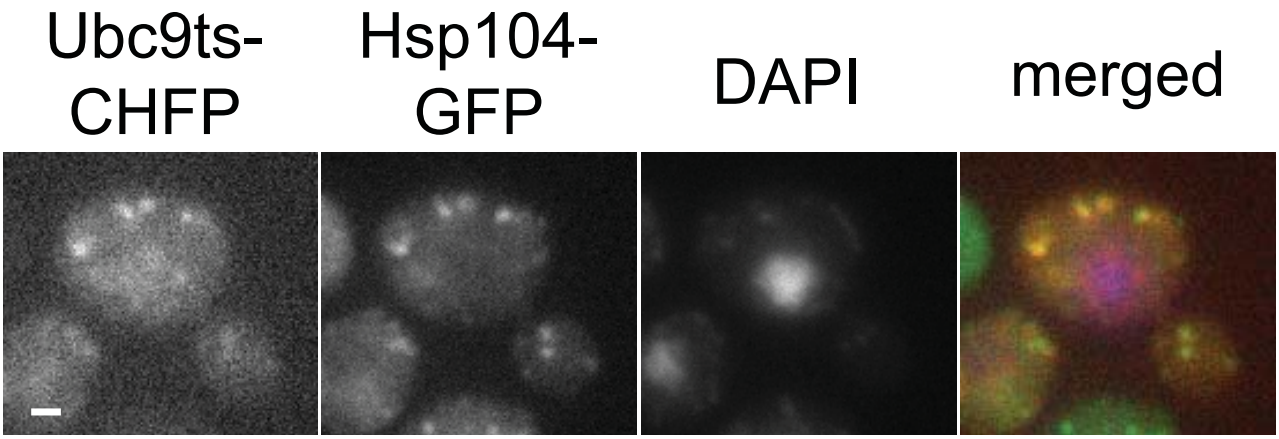

Figure S4 Hsp104 does not colocalize with perinuclear Q-bodies. Images of a fixed cell expressing Hsp104-GFP (green) and Ubc9ts-CHFP (red) and stained with DAPI (blue) after a 15 min shift from 28°C to 37°C. Merged represents the overlay of the three channels. Scale bar equals 1 μm.

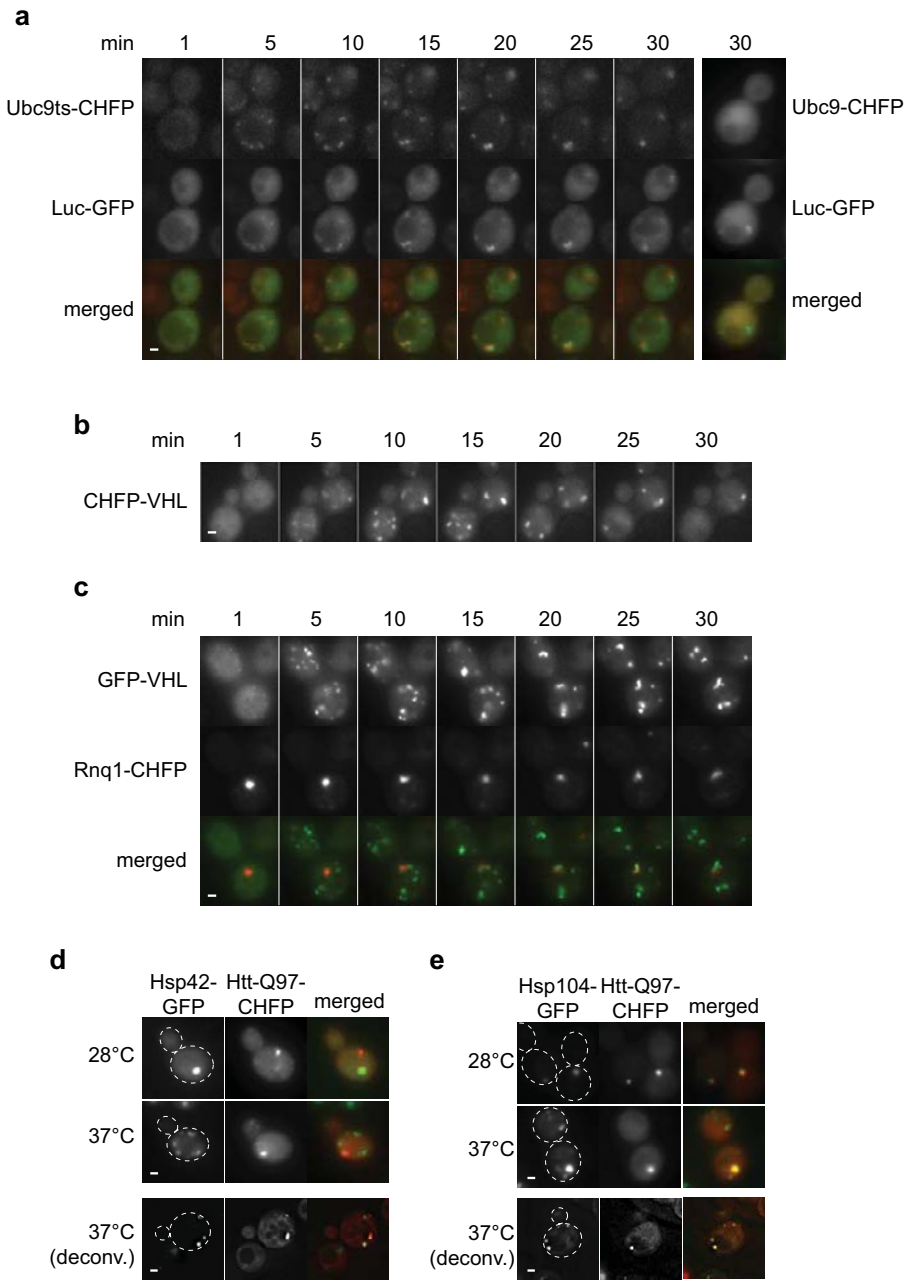

Figure S5 Different types of misfolded proteins, but not amyloids, co-localize to and are processed together via the same Q-bodies. (**a**) WT cells expressing Ubc9ts-CHFP and Luc-GFP were grown at 28°C in galactose medium and imaged at 37°C in glucose medium. 5 min series of images show Ubc9ts-CHFP in red and Luc-GFP in green. Cells expressing Ubc9-GFP were similarly prepared and imaged 15 min after the shift. Scale bar equals 1 μm. (**b**) WT cells expressing CHFP-VHL were grown as in **a**. 5 min series of images shows CHFP-VHL over 30 min. Scale bar equals 1 μm. (**c**) WT cells expressing GFP-VHL (green) and Rnq1-CHFP (red) were grown and imaged as in **a**. Scale bar equals 1 μm. (**d**) Cells expressing Hsp42-GFP and Htt-Q97-CHFP were grown at 28°C in galactose medium and shifted for 10 min at 37°C in glucose medium. Two-color images (deconvolved in the lower panel) show Hsp42-GFP signal in green and Htt-Q97-CHFP signal in red. Scale bar equals 1 μm. (**e**) Cells expressing Hsp104-GFP (green) and Htt-Q97-CHFP (red) were grown and imaged as in **d**. Scale bars equal 1 μm.

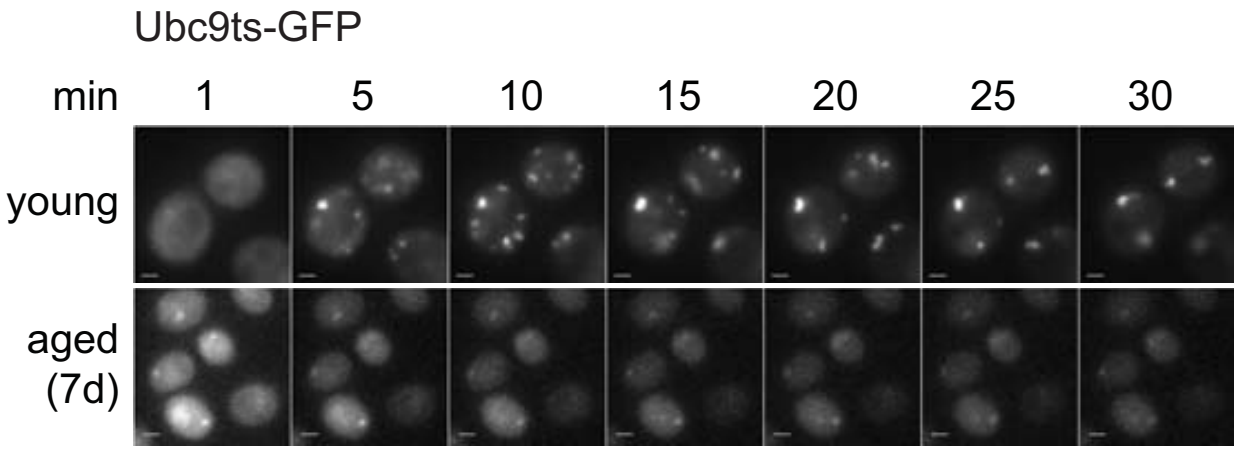

Figure S6 Aging impairs the Q-body pathway. Cells expressing Ubc9ts-GFP were grown at 28°C for 5 hours (young) or for 7 days (aged) and imaged at 37°C. 5 min series of a 30 min movie show the GFP signal. Scale bars represent 1 µm.

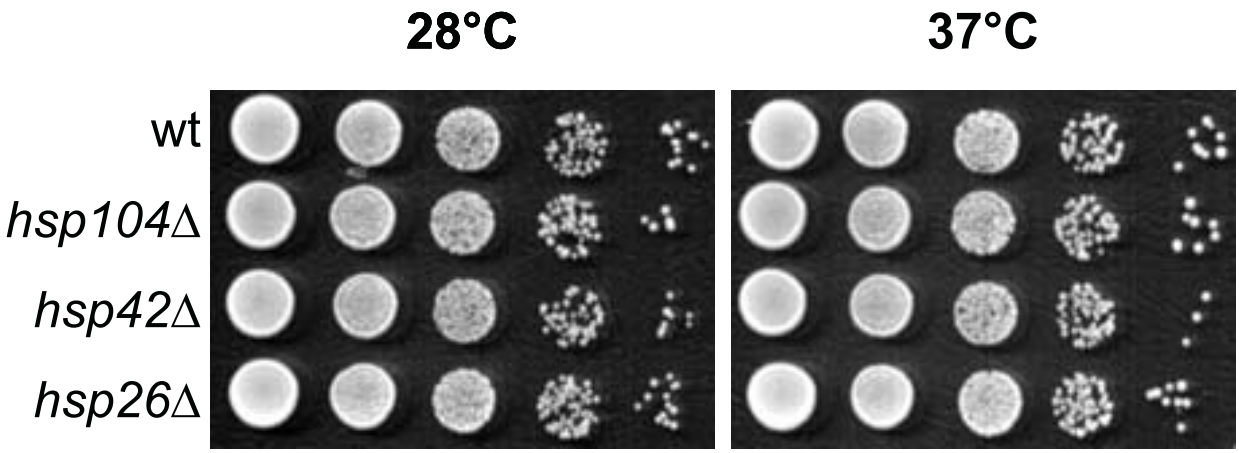

Figure S7 Deletion of Hsp42, Hsp26 or Hsp104 does not cause any appreciable growth defects at 37°C. A suspension of WT, *hsp104*Δ, *hsp42*Δ, and *hsp26*Dcells were serially diluted and dropped on YPD at 28°C and 37°C.

Fig. 1d

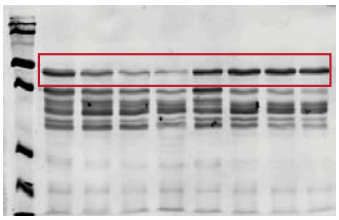

Fig. 3f

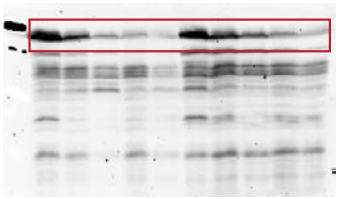

Fig. 4b

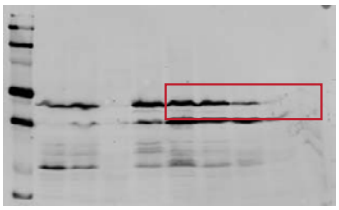

Fig. 4b

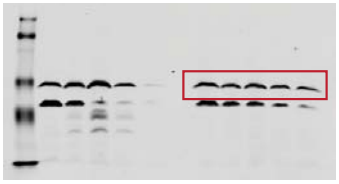

Fig. 4b

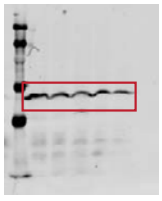

Fig. 5f Fig. 4b

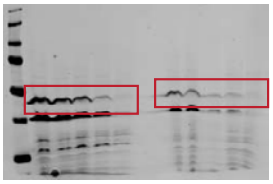

Fig. 4b

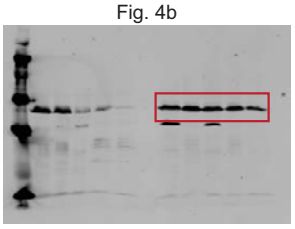

Fig. 5f

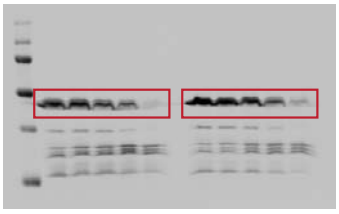

Fig. 5f

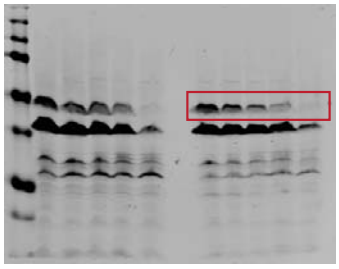

Fig. 5f

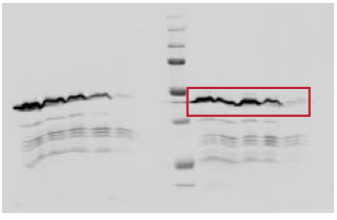

Fig. S1b

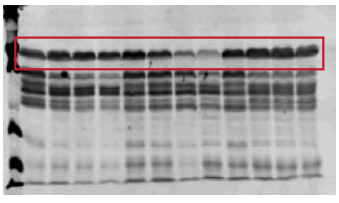

Figure S8 Full scans of original immunoblot data presented in this study. Red outlines represent the immunoblot sections presented in the corresponding main figures.

Supplementary Table:

Table 1: Chaperones involved in the Q-body pathway organized by family and corresponding yeast names. Previously described activities and phenotypes of each chaperone family in the Q-body pathway are included.

Supplemental Video Legends

Video S1: Misfolded Ubc9ts forms Q-bodies. Live-cell movie of Ubc9ts-GFP in a WT cell at 37°C. Interval between frames is 15 s. Total time of acquisition was 30 min. Refers to Fig. 1f.

Video S2: Actin cytoskeleton does not affect the Q-body pathway. Live-cell movie of cells expressing Ubc9ts-GFP (left panel) or Abp1-GFP (right panel) at 37°C with (lower panel) or without (upper panel) LatA treatment. Interval between frames is 15 s. Total time of acquisition was 30 min. Refers to Fig. 2a.

Video S3: The Q-body pathway is energy dependent. Live-cell movie of Ubc9ts-GFP in WT cell at 37°C with (right panel) or without (left panel) sodium azide and deoxyglucose (Az/Deox) treatment. Interval between frames is 15 s. Total time of acquisition was 30 min. Refers to Fig. 2d.

Video S4: Q-bodies localize in proximity to the cortical ER. 3D projection of a live-cell expressing Ubc9ts-CHFP Q-bodies (red) and Rtn1-GFP (green, cortical ER) at 37°C. 0.2 µm intervals. Refers to Fig. 3c.

Video S5: The Q-body pathway depends on an intact cortical ER. Live-cell movie of Ubc9ts-GFP in WT and *rtn1Δrtn2Δyop1Δ* cells at 37°C. Interval between frames is 15 s. Total time of acquisition was 30 min. Refers to Fig. 3e.

Video S6: Hsp70 is required for Q-body formation, dynamics and clearance. Live-cell movie of Ubc9ts-GFP in WT, *ssa1*D*ssa2*Δ and *sse1*Δ cells at 37°C. Interval between frames is 15 s. Total time of acquisition was 30 min. Refers to Fig. 4c and h.

Video S7: Hsp82 is required for Q-body maturation and clearance. Live-cell movie of Ubc9ts-GFP in *HSP82* and *hsp82ts* cells at 37°C. Interval between frames is 15 s. Total time of acquisition was 30 min. Refers to Fig. 4e.

Video S8: Ydj1 participates in the formation and localization of Q-bodies. Live-cell movie of Ubc9ts-GFP expressed in *ydj1*Δ cells with an empty vector, *YDJ1*, or *ydj1(C406S)* at 37°C. Interval between frames is 15 s. Total time of acquisition was 30 min. Refers to Fig. 4g.

Video S9: **Hsp104 co-localizes with peripheral Ubc9ts-forming Q-bodies**. Live-cell movie of a cell co-expressing Ubc9ts-CHFP (red) and Hsp104-GFP (green) at 37°C. Interval between frames is 15 s. Total time of acquisition was 60 min. Refers to Fig. 5a.

Video S10: Q-body pathway relies on the balance between Hsp104 and Hsp42 activities. Live-cell movie of Ubc9ts-GFP in WT, *hsp104*Δ, *hsp42*Δ, and *hsp42*D*hsp104*Δ cells at 37°C. Interval between frames is 15 s. Total time of acquisition was 30 min. Refers to Fig. 5d and g.

Video S11: VHL, but not Htt-Q97, is concentrated to Q-bodies. Live-cell movie of Ubc9ts-GFP (green) co-expressed with CHFP-VHL (red) or Htt-Q97-CHFP (red) in WT cell at 37°C. Interval between frames is 15 s. Total time of acquisition was 30 min. Refers to Fig. 6a and b.

Video S12: TOR signaling regulates the Q-body pathway. Live-cell movie of Ubc9ts-GFP in WT cell with or without 0.2 µg/mL rapamycin (Rap) treatment at 37°C. Total time of acquisition was 30 min. Refers to Fig. 7c.